Transportation Geotechnics 52 (2025) 101586

Contents lists available at ScienceDirect

Transportation Geotechnics

journal homepage: www.elsevier.com/locate/trgeo

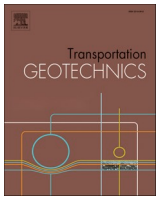

Deformation properties and performance evaluation of reused ballast with waste tire-derived aggregates

Stanislav Lenart, Siva Ram Karumanchi *

Department of Geotechnics, Slovenian National Building and Civil Engineering Institute (ZAG), Ljubljana, Slovenia

ARTICLE INFO

Keywords:
Reused ballast
Rubber
Cyclic simple shear tests
BBI
Degradation

ABSTRACT

The present study evaluates the shear strength characteristics, deformation properties, and degradation behavior of limestone-based reused ballast (RB) material by mixing crumbs of waste tire-derived aggregates (TDA), focusing on its suitability for railway infrastructure. Conventional large-scale direct shear tests and novel large-scale cyclic simple shear tests were performed to investigate the effects of tire-derived aggregate (TDA) content, with particle sizes varying between 22.4 mm and 50 mm. The results indicate that adding 5 % by the mass of TDA slightly reduced the friction angle from 46.6° to 44.5°, which is not a significant change compared to RB. However, increasing the TDA content to 10 % led to a notable decrease in the friction angle to 41°, highlighting the significant impact of higher TDA content on the shear strength behavior. Further, incorporating 5 % TDA improved the shear modulus and damping ratio relative to RB, which is attributed mainly to the similar larger particle sizes (22.4–50 mm) of TDA. Conversely, at 10 % TDA content, reductions in both shear modulus and damping ratio were observed. The ballast breakage index (BBI), evaluated through cyclic simple shear tests, showed a significant decrease from 15 % for RB to 9.5 % for the ballast sample containing 5 % TDA. Additionally, increased TDA content enhanced material durability, reducing Los Angeles abrasion (LAA) losses from an initial 33.5 to under 30 % at 5 % TDA. These findings demonstrate that incorporating 5 % by mass of TDA into RB material is optimal for enhancing deformation characteristics and reducing ballast degradation while maintaining adequate shear strength. This sustainable approach facilitates the recycling of waste materials, promotes a circular economy, and helps maintain safe and stable railway track conditions.

Introduction

In recent decades, rail transportation systems have advanced significantly with the development of sustainable railway infrastructure, the expansion of freight corridors, and the development of high-speed railways. Driven by the need to enhance railway performance and reduce capital construction costs, these advancements have encouraged the adoption of alternative designs and new construction methodologies. Most railway infrastructure relies on ballast tracks, which exhibit three major roles: (i) they uniformly transmit the trainload to the underlying subgrade, (ii) they uphold track geometry and alignment, and (iii) they function as a drainage barrier [1]. The persistent influence of train loads and varying environmental conditions leads to substantial ballast degradation [2,3]. The progressive degradation of ballast leads to an increased generation of fines. The accumulation of these fines generated from particle breakage and degradation contributes to void filling, reducing the drainage capacity of the ballast material [4]. Moreover, ballast particles undergo densification and rearrangement beneath the sleepers under repeated train loads. This densification forces particles to flow outward, reducing internal friction characteristics and lateral confinement and leading to increased vertical and horizontal deformations. Consequently, reduced deformation characteristics of ballast compromise track stability, ultimately resulting in track geometry defects [5]. Therefore, addressing ballast degradation is necessary to enhance the stability and serviceability of railway tracks, thereby minimizing maintenance costs. Accordingly, numerous studies [4,6–11] have concentrated on the implementation and maintenance of these ballast track systems. Previously, various techniques have been implemented to improve the serviceability of railway ballast, including geogrid and geocell reinforcement [12–15], modified ballast materials [11,15–18], under sleeper pads [19–22], and under ballast mats [23,24].

The ballast will inevitably degrade after an operational period, requiring the replacement or addition of newly sourced material from

* Corresponding author.
E-mail addresses: stanislav.lenart@zag.si (S. Lenart), ram.karumanchi@zag.si (S.R. Karumanchi).

https://doi.org/10.1016/j.trgeo.2025.101586
Received 7 February 2025; Received in revised form 14 May 2025; Accepted 15 May 2025
Available online 16 May 2025

Table 1
Summary of relevant literature on the Ballast materials and TDAs.

Reference/Year	Ballast materials	TDA (%)	TDA size (mm)	Key Findings	Relevance
[38] (2025)	Fresh andesite igneous rock, TDA	2.5–12.5 %	1–30 mm	Developed ballast mechanical properties index (MPI).	Low to medium particle size TDA. Monotonic and cyclic direct shear tests.
[39] (2024)	Rubber intermixed ballast systems (RIBS)	0–15 %	9.5–19 mm	The stress reduction of 20–30 % at the lower ballast layer with the addition of TDA-10 %. Decrease of peak friction angle with an increase in rubber content.	Lower particle size of TDA, Large-scale monotonic and cyclic triaxial tests to evaluate the permanent deformation behavior.
[40] (2024)	Fresh and recycled slag ballast	–	–	An increase in maximum ballast size raised the BBI by more than 10 %; recycled ballast reduced the BBI by upto 7 %.	Cyclic and post-cyclic monotonic Large-scale triaxial tests to evaluate the permanent deformation behavior.
[41] (2024)	Fresh Granite Ballast, (CR)	0–15 %	9.5–19 mm	Lower BBI $<$ 0.1 after adding 5 % or more rubber. Track vibrations were minimized by 60 % for TDA-10 % by volume compared to conventional ballast.	Lower particle of TDA, Large-scale monotonic and cyclic triaxial tests, field prototype study.
[42] (2024)	Quarried gneiss granular aggregate, CR	10 %	0.8–3 mm 3 to 7 mm	Crumb rubber content at 10 % by mass is nearly double that at 10 % by volume.	Packing tests to evaluate segregation, differences in % mass and % volume addition crumb rubber
[43] (2023)	TDA	100 %	6.4–12.7 mm	Rubber aggregate enhances energy dissipation but reduces peak stress.	Small-scale cyclic simple shear tests and bender element tests to evaluate the shear modulus and damping ratio
[44] (2022)	Well-graded sand and gravel, TDA	0–100 %	11–12 mm 5–6 mm 2–3 mm	TDA chips enhance the sub-ballast strength, while TDA granules negatively affect it. Recommended optimum tire content of 20 %.	Particle size of TDA limited to 12 mm, Large-scale monotonic and cyclic triaxial tests.
[45] (2022)	Fresh basalt ballast, CR	10 %	12.5–25 mm 4.75 to 9.5 mm	The prominent effect of smaller-size crumb rubber in affecting the damping properties of degraded ballast.	Particle size of TDA limited to 25 mm, Drop-weight impact loading tests to evaluate the damping, stiffness and degradation properties
[46] (2021)	Coal fouled ballast	0–40 %	9–26.5 mm (gradation of coal foul ballast)	Ballast shear strength and dilatancy decrease with higher normal pressure and fouling.	Monotonic large scale direct shear tests.
[47,48] (2019)	Fresh granite ballast, TDA	0–10 %	20–63.5 mm	Adding 5 % rubber caused about 10 % reduction in shear resistance and modulus, but increased damping ratio by over 15 %.	Large-scale monotonic and cyclic direct shear tests.
[49,50] (2018,2017)	TDA	100 %	75–100 mm (Type A) 150–300 mm (Type B)	The shear modulus of Type B TDA (maximum 2,386 kPa) decreases with higher shear strains, similar to natural granular soils but with lower magnitudes.	Larger particle size of TDA. Large-scale cyclic simple shear tests (with cyclic strain limit ranging from 0-10 %) and large-scale direct shear tests.
[29,51] (2016)	Dolamite ballast, TDA	0–30 %	19–63.5 mm	Based on the combined effects on shear strength and settlement behavior, 10 % TDA is proposed as optimal.	Ballast deformation behavior and particle breakage were assessed through cyclic loading tests in ballast box.
[52] (2015)	Fresh granite ballast, CR	0–30 %	8–22.4 mm	Crumb rubber content of 10 % is optimal, as higher amounts (20–30 %) can worsen track geometry, whereas 10 % reduces ballast breakage without increasing settlement.	Ballast box tests to evaluate the influence of the quantity of crumb rubber
[53] (2005)	Fresh ballast	–	–	Ballast experiences severe breakage at low confinement ($\leq$30 kPa), whereas slight increases in confinement notably reduce particle degradation.	Large scale triaxial tests and developed ballast breakage index to evaluate degradation under cyclic loading

Table 2
Summary of large-scale laboratory tests performed in literature for the mechanical characterization of ballast material.

Large-scale experimental tests in Laboratory	Test Type	Dimensions	Measurements	References
Triaxial Test	Static and cyclic	Dia-300 mm, H-600 mm	Permanent axial deformation, volumetric strain, resilient modulus, damping ratio and BBI	[36,53,58]
	Cyclic and post-cyclic monotonic		Permanent axial deformation, shear modulus, damping ratio, friction angle, fouling index	[40]
	Cyclic	Dia-300 mm, H-600 mm	Dynamic characteristics of tyre derived aggregates	[65]
	Static and cyclic	Dia-305 mm, H-610 mm	Permanent axial deformation of dry and wet ballast	[59]
Direct Shear Test	Static	(LxWxH) 500x500x350 mm	Stress–strain, friction angle, cohesion, BBI	[48]
	Static and cyclic		Stress–strain, friction angle Interface shear modulus, Damping Ratio	[47]
	Static	(LxWxH) 450x450x300 mm	Friction angle, Interface efficiency factor, BBI	[30]
	Static	(LxWxH) 600x700x550 mm	Shear and deformation characteristics	[62]
Cyclic Simple Shear test	Cyclic	(LxWxH) 3048x1219x1400 mm	Shear Modulus and Damping ratio	[49]
Ballast Box Test	Track Process Simulation (TPSA)	(LxWxH) 800x600x600 mm	Lateral deformation, shear and volumetric response	[71]
	Cyclic	(LxWxH) 300x700x450 mm	Lateral deformation, shear and volumetric response	[22]
Plate Load test	Static	(LxWxH) 800x600x400 mm	Ballast settlement and stiffness, BBI	[17]
Impact tests	Impact Loading	Dia-300 mm, H-560 mm	Vertical and lateral deformation, Impact forces, BBI	[24]
		Dia-240 mm, H-500 mm	Degradation and morphological indices	[3]
			Stiffness and Damping	[45]

quarries. In the last three decades, igneous or metamorphic rocks like granite have been the preferred choice for ballast because of their superior durability over sedimentary rocks [25]. However, the limited availability of high-quality ballast in many countries [25,26] has prompted them to use alternatives such as limestone [25], recycled materials from foamed glass [27], ballast with tire derivatives [16,28,29], and geosynthetic reinforced ballast [30–32]. Additionally, a trend has been increasing to conserve high-quality raw materials by incorporating recycled materials [33,34]. Indraratna et al., [35] indicated that incorporating a rubber tire assembly into the load-bearing substructure and adding tire arc segments along the track shoulders increased the ballast layer's confinement, thereby reducing settlements and lateral displacements. Numerous studies [4,11,15,17,35–37] have been undertaken to examine various innovative strategies for utilizing recycled industrial wastes, such as tire derivatives, coal wash, plastics, and glass, aiming to mitigate track degradation and elevate overall performance. The findings from these studies suggest that modified ballast with tire-derived aggregates (TDA) consistently shows improved performance. Table 1 presents a comprehensive review [29,38–53] of the findings and implications derived from relevant studies, detailing various ballast and TDA materials. It specifically addresses the impact of the percentage of TDA addition and its particle size on the mechanical properties of these modified ballast materials. This systematic review of recent literature contributes to a deeper understanding of the factors influencing the performance of ballast materials in this context. Notably, adding waste tire chips reduces particle breakage compared to pure ballast. However, the stress–strain behavior observed from the static and cyclic loading tests indicated that TDA addition significantly decreased the peak shear stress, internal friction angle, dilation, and interface shear stiffness [47]. While most studies [28,29,52,54,55] used TDA sizes between 8 and 24 mm, Song et al. [47] used particle sizes between 8 and 63.5 mm for TDA in the ballast mix. Anjos et al. [42] observed aggregate segregation in the case of smaller sizes of crumb rubber. In particular, they observed increased segregation of smaller-sized crumbs at the bottom due to cyclic loads. This indicated that the use of a larger particle size of TDA could reduce the particle segregation at the bottom of modified railway ballast material.

Railway traffic exerts compressive as well as shear loads on the ballast and subgrade. Vertical and shear stresses in the ballast tracks are interconnected, influencing each other in complex ways [56]. High vertical stresses may enhance friction between ballast particles, aiding in shear resistance. However, if vertical stresses become excessive, they can wear down the ballast, weakening its shear resistance. A comprehensive understanding of prior research studies [47,57–60] indicates that evaluating the deformation behavior of ballast materials requires large-scale laboratory experiments. These experiments include large-scale direct shear tests [46–48,50,61,62], large-scale triaxial tests [57–59,63–65], ballast box tests [22,57], and prototype testing [23,24,63,66]. In addition, Los Angeles abrasion (LAA) tests [26,67–69], and Micro-Deval abrasion (MDA) tests [26,67] are performed to evaluate the degradation of ballast materials. Table 2 summarizes the application methods of these large-scale tests and their dimensions, which range from a minimum of 300 × 300 × 100 mm to a maximum of 800 × 500 × 100 mm. Most research [17,39,57,59,70] on fine and coarse-grained materials and ballast-TDA mixtures has focused on compression behavior involving various uniaxial and triaxial compressive tests. The direct shear test is widely used to reveal various properties of granular and fine materials. Monotonic large-scale direct shear and triaxial tests evaluate ballast material's shear strength characteristics [47,58,61]. Cyclic triaxial tests, on the other hand, are used to evaluate the resilient and permanent deformation behavior of ballast, focusing on shear stiffness, dissipated energy, and damping ratio [71,72]. Besides, monotonic and cyclic direct shear tests are also used to assess the frictional characteristics, compressive behavior, interface shear stiffness, and damping ratio [47]. Over the years, numerous laboratory tests have been established to estimate the resilience and deformation behavior of both fine-grained and coarse-grained materials. Notably, cyclic triaxial and cyclic simple shear tests are frequently used in laboratories to evaluate the cyclic behavior of fine-grained materials. The cyclic triaxial test is extensively used to assess the cyclic behavior of coarse-grained ballast materials because it allows for the consolidation of specimens under isotropic or anisotropic conditions, thus simulating *In situ* ground conditions [73]. Alternatively, the cyclic simple shear test also provides a more realistic representation of stress conditions in the horizontal plane characterized by maximum shear stress, closely matching those at the *In situ* ground conditions [43,73,74].

The primary concern of this research is the lack of high-quality ballast material, as highlighted by existing studies [25,26]. Given the growing reliance on low-durability limestone ballast in regions with a limited high-quality ballast material, a thorough analysis of its

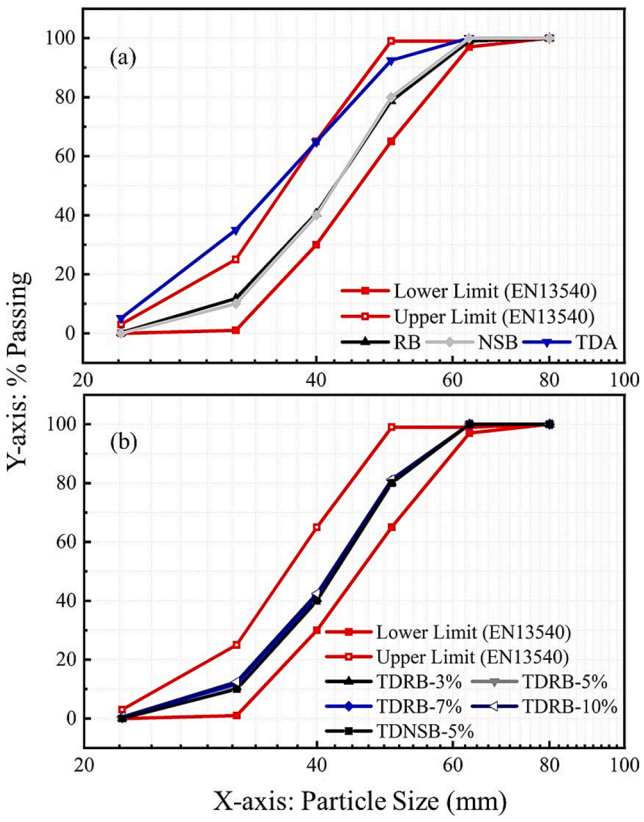

Fig. 1. Gradation curves a) RB, NSB, and TDA b) TDRB and TDNSB-5% mixtures.

properties and potential improvements from the addition of waste tire-derived aggregates is essential. In this regard, the present study is focused on evaluating the deformation properties and mechanical degradation of these modified materials through a comprehensive series of mechanical tests. The objective of this evaluation is to contribute to the existing research knowledge regarding the shear strength, deformation, and degradation characteristics and potential applications of these materials in railway infrastructure. Railway ballast experiences complex loading from train movements, including vertical and shear forces, which impact its deformation behavior. As discussed in Tables 1 and 2, researchers have successfully characterized ballast shear strength and deformation properties using static and cyclic triaxial tests, ballast box tests, and direct shear tests, providing valuable insights into ballast performance. There exists a significant need for further research into the cyclic shear behavior of railway ballast, which is vital for a thorough understanding of deformation behavior and material degradation. Additionally, it is important to highlight that the shear modulus derived from cyclic direct shear tests primarily reflects the interface shear stiffness and may not accurately represent the overall shear stiffness of the ballast materials. Addressing these aspects could enhance our understanding and improve the performance of railway ballast. This study introduces a novel experimental approach by implementing large-scale cyclic simple shear testing for railway ballast material to analyze the shear response of recycled limestone ballast-TDA mixtures under repeated loading cycles. Unlike conventional cyclic triaxial shear tests, cyclic simple shear testing replicates the shear stresses that ballast experiences due to cyclic wheel-rail interactions. These shear forces contribute to ballast degradation, track misalignment, and differential settlement, making their accurate assessment of modified ballast behavior and mitigating maintenance costs. A novel large-scale cyclic simple shear apparatus has been designed and developed in the geotechnical laboratory at the Slovenian National Building and Civil Engineering Institute (ZAG), Slovenia, to evaluate the cyclic shear behavior of ballast materials. The presented research primarily focuses on cyclic shear loading and unloading, evaluating the material's response to repeated shear strains, as well as its stiffness and damping behavior. In addition, monotonic direct shear tests were performed to explore the influence of the TDA content on the shear strength characteristics of fresh and recycled limestone-based ballast. Furthermore, this study presents the evaluation of ballast degradation using the ballast breakage index (BBI), Los Angeles abrasion (LAA), and Micro-Deval abrasion (MDA) tests. The findings provide insights into the deformation and degradation properties of reused limestone-based ballast and TDA mixed reused ballast material, promoting sustainability in railway infrastructure.

Objective and scope of the study

The primary objective of this study is to evaluate the mechanical and shear characteristics of limestone-based reused ballast (RB) material by adding shredded waste tire-derived aggregates (TDA) with particle sizes ranging from 22.4-50 mm. The objectives include 1) assessing the shear strength characteristics of reused ballast (RB) and the potential changes in TDA mixed reused ballast material (TDRB), 2) analyzing the deformation properties from cyclic simple shear tests, including shear stiffness and damping properties of RB and TDRB mixtures, 3) evaluating the particle breakage of RB and TDRB mixtures induced from the cyclic simple shear from ballast breakage index (BBI), and 4) assessing the ballast degradation from Los Angeles abrasion (LAA), and Micro-Deval abrasion (MDA) tests. The stress–strain response, internal friction angle, dilation behavior, shear stiffness, and damping ratio of RB and TDRB were analyzed to understand the influence of TDA. Additionally, monotonic direct shear tests were conducted on the freshly sourced limestone-based ballast material (NSB) and a mixture of freshly sourced ballast with 5 % TDA (TDNSB-5 %) to assess its shear strength characteristics compared to RB and TDRB mixtures. Finally, the optimal combination of TDRB ballast mixture for railway track application was recommended.

Materials and laboratory testing program

The recycled ballast material, sourced from the Slovenian railway network, was initially derived from limestone [25]. To ensure it was clean before testing, the selected recycled ballast was initially washed and dried, followed by sieving with appropriate sieves to obtain the particle size gradation. The 100 % recycled tire-derived aggregates (TDA), supplied by a local company, were primarily sourced from the tires of heavy vehicles. These tires were shredded into rubber aggregates after removing the fibers and thin steel wires. Fig. 1(a) presents the gradation curves of the RB, NSB, and TDA materials. The reused ballast (RB) was obtained from existing railway tracks, which resulted in distinct morphological differences compared to newly sourced ballast (NSB). RB particles were more rounded and had smoother surfaces due to previous operational loading and abrasion, while NSB particles retained sharper edges and rougher textures. The particle size distribution of TDAs ranges from 22.4 to 50 mm, with a mean particle size (D_{50}) of 35 mm. This indicates that TDAs were relatively larger compared to those used in previous studies, as shown in Table 1. The larger size was intended to prevent rubber particle segregation in the mixtures, similar to the usual particle size of ballast material. Accordingly, the overall particle size distribution curves of the TDRB and TDNSB-5 % mixtures, as shown in Fig. 1(b), were in accordance with the gradation recommended for ballast material by European standards [75]. The TDRB ballast mixtures for monotonic and cyclic tests were manually prepared by mixing recycled ballast with TDA in proportions ranging from 0 % to 10 % by mass. Adding the TDA content by over 10 % by mass can significantly increase the volume of the rubber material in the ballast mixture. This may lead to reduced stiffness in the ballast system, causing unacceptable settlements [29,54,55]. Therefore, in the present study,

Table 3
Initial and relative densities of ballast materials.

Sample	TDA content % by mass	Initial Density	Relative Density
	%	kg/m^3	
RB	0	1553	1
TDRB-3 %	3	1480	0.95
TDRB-5 %	5	1410	0.91
TDRB-7 %	7	1348	0.87
TDRB-10 %	10	1293	0.83
NSB	0	1463	1
TDNSB-5 %	5	1373	0.94

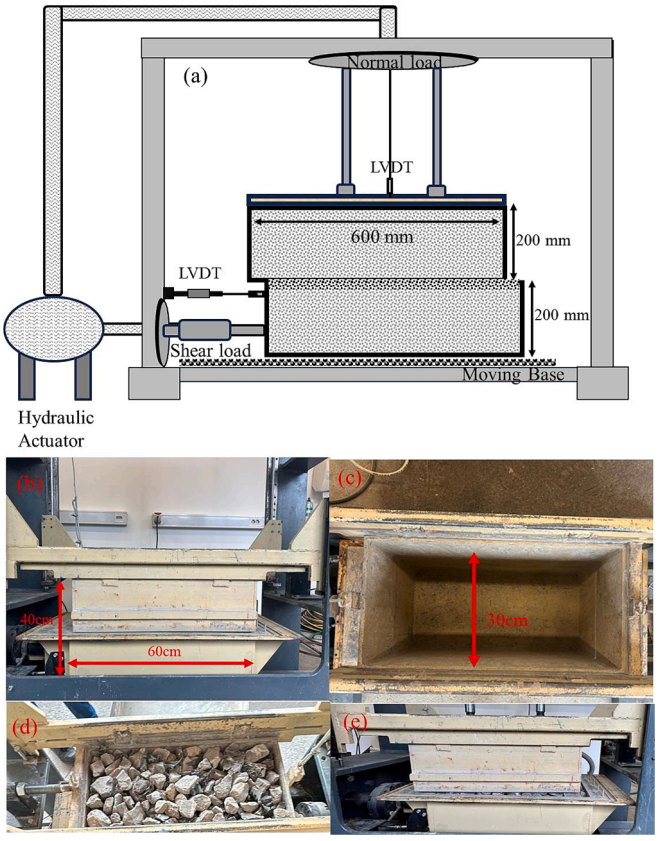

Fig. 2. Illustration of (a) Direct shear test (a) Front view (b) Top view (c) Sample preparation (d) shearing of 10 cm.

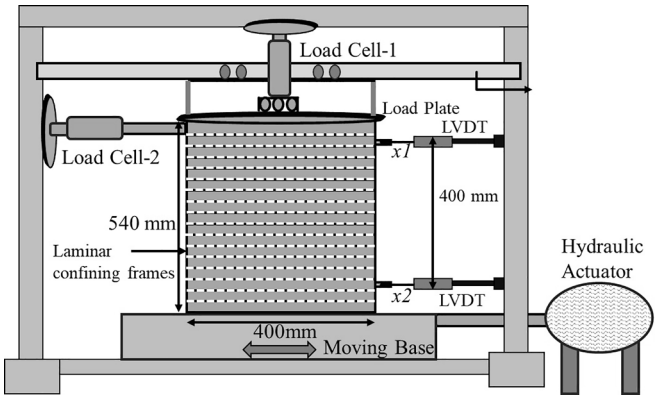

Fig. 3. Schematic illustration of the cyclic simple shear test setup.

the highest percentage of TDA by mass proportion was limited to 10 % by mass. Table 3 summarizes the initial and relative density values of the RB and TDRB mixtures. The relative densities of the TDRB and TDNSB mixtures were estimated using their corresponding pure ballast specimens as reference points. The RB specimen showed the highest initial density (1553 kg/m^3), followed by NSB (1463 kg/m^3), while TDRB-10 % had the lowest initial density at 1293 kg/m^3. The reused ballast samples underwent oven and air-drying to ensure dryness before preparing the specimens for monotonic and cyclic shear tests.

Large-scale direct shear test

The schematic illustration of the setup dimensions and loading arrangement of the large-scale direct shear test setup is shown in Fig. 2 (a). The monotonic direct shear tests for each specimen, RB, TDRB-3 %, TDRB-5 %, TDRB-7 %, TDRB-10 %, NSB, and TDNSB-5 % were performed at four different normal pressures: 50, 100, 200, and 300 kPa. As shown in Fig. 2(b)-()–(d))–(, the samples were prepared in two split boxes (top and bottom), with each box having dimensions of 600 × 300 × 200 mm (L × W × H). The specimens within these boxes were compacted to achieve their respective densities, as detailed in Table 3. The displacement transducer, attached to the lower frame (Fig. 2(e)), enabled the measurement of the relative displacement between the bottom and top split boxes. The monotonic shearing process was carried out at a constant speed of 2.5 mm/min, continuing until either failure occurred or a maximum shear displacement of 10 cm was achieved. Special care was taken in measuring displacements and shear loads to ensure precise evaluation of recorded data across the full range of displacements. Each test involved measuring vertical and horizontal forces to calculate shear and normal stress, along with horizontal and vertical displacements. Through these tests, the relationships between shear stress and horizontal displacement, as well as vertical and horizontal displacement during shearing, were established to evaluate the behavior of RB, TDRB, NSB, and TDNSB-5 % mixtures. Moreover, these measurements were used to calculate the internal friction angle of all the tested samples.

Large-scale cyclic simple shear tests

The multi-functional large-scale testing equipment shown in Fig. 3 consisted of a uni-directional moving base, a frame setup for applying normal and horizontal loads, hydraulic vertical and horizontal actuators, load cells, and advanced data acquisition systems. Key features include a 100 mm displacement capacity for the movable base and a load measurement range of 0–200 kN for normal and horizontal loads, with the added capability to apply and measure cyclic displacements and loads with the capability of measurements at large strains and small strains ranging as small as 10^{-4} %. This versatile setup supports various tests, such as large-scale triaxial, direct shear, and cyclic simple shear tests. Cylindrical specimens are usually preferred in triaxial tests because their symmetrical shape allows for uniform stress distribution and consistent application of confining pressure and axial load [73]. However, for large-scale shear tests cylindrical samples present challenges due to the less defined shear plane, which complicates the application of uniform shear stress. Therefore, rectangular specimens were chosen for large-scale simple shear tests in this study, as they provide a well-defined and consistent shear plane, facilitating the uniform application of shearing. In developing the dimensions, laminar confining frames, and loading setup for the cyclic simple shear tests, the following considerations were prioritized: First, the height of the laminar box should be designed large enough to support large-scale testing of ballast specimens. Accordingly, the overall dimensions of the specimens for cyclic simple shear tests were selected based on the research knowledge obtained from the extensive review, as shown in Table 2. The adopted dimensions were 400 × 400 × 540 mm (L × W × H). Second, the thickness of the laminar confining frames had to be

Fig. 4. Pictures of cyclic simple shear test (a) Experimental arrangement (b) Displacement transducer (c) Sample preparation (d) Sample preparation in apparatus (e) Degraded material after the test.

Table 4
Cyclic testing protocol adopted in cyclic simple shear tests.

Stage	Loading Cycle	Strain	Loading frequency	Amplitude	Loading rate
		%	Hz	mm	mm/sec
1	1–3	0.0005	0.0167	0.0019	0.000125
2	4–6	0.004	0.0167	0.015	0.001
3	7–9	0.016	0.0167	0.06	0.004
4	10–12	0.065	0.0167	0.24	0.016
5	13–15	0.130	0.0167	0.48	0.032
6	16–18	0.25	0.0167	0.96	0.064
7	19–21	1.00	0.0167	3.83	0.25
8	22–24	2.00	0.0167	7.66	0.51
9	25–27	4.00	0.0167	15.32	1.02

sufficient to allow for distinct shearing at each plane and ensure the evaluation of more precise shear deformations even at low-frequency loading. Hence, the thickness of each frame was considered 3 cm. Lastly, the top loading arrangement is needed to promote sliding and should eliminate the probable tilting of frames during the shearing process. To accommodate this, the movement assisting girder was provided at the top, as illustrated in Fig. 3. The gap between the laminar frames was provided with flexible Teflon sheets to ensure smooth sliding between the frames and, with the assistance of the moving assistant girder, eliminate the tilting of the frames. All these considerations ensure that the equivalent shear-beam deformation mode can be sustained. While Teflon sheets were employed between the frames to reduce friction, a minor residual frictional component may inevitably exist. The consistent experimental conditions across all tests suggest that any residual friction was minimal, uniform, and, therefore, unlikely to significantly affect the comparative evaluation of the tested ballast mixtures. The developed large-scale cyclic simple shear test setup, as shown in Figs. 3 and 4(a), comprises 18 rectangular aluminum frames, each having dimensions 420 × 420 × 30 mm (L × W × H), resulting in a total height of 540 mm. The inner side-to-side distance of the frame was 400 mm. As shown in Fig. 4(a), the inner wall of the laminar box was installed with a fabric membrane to prevent the loss of fine particles during the test.

Lackenby et al. [76] have shown that the vertical stress levels experienced by ballasted railway tracks can vary significantly, typically ranging from 200 kPa to 1250 kPa. This variation is influenced mainly by the type of train operating on the tracks, with heavier and faster

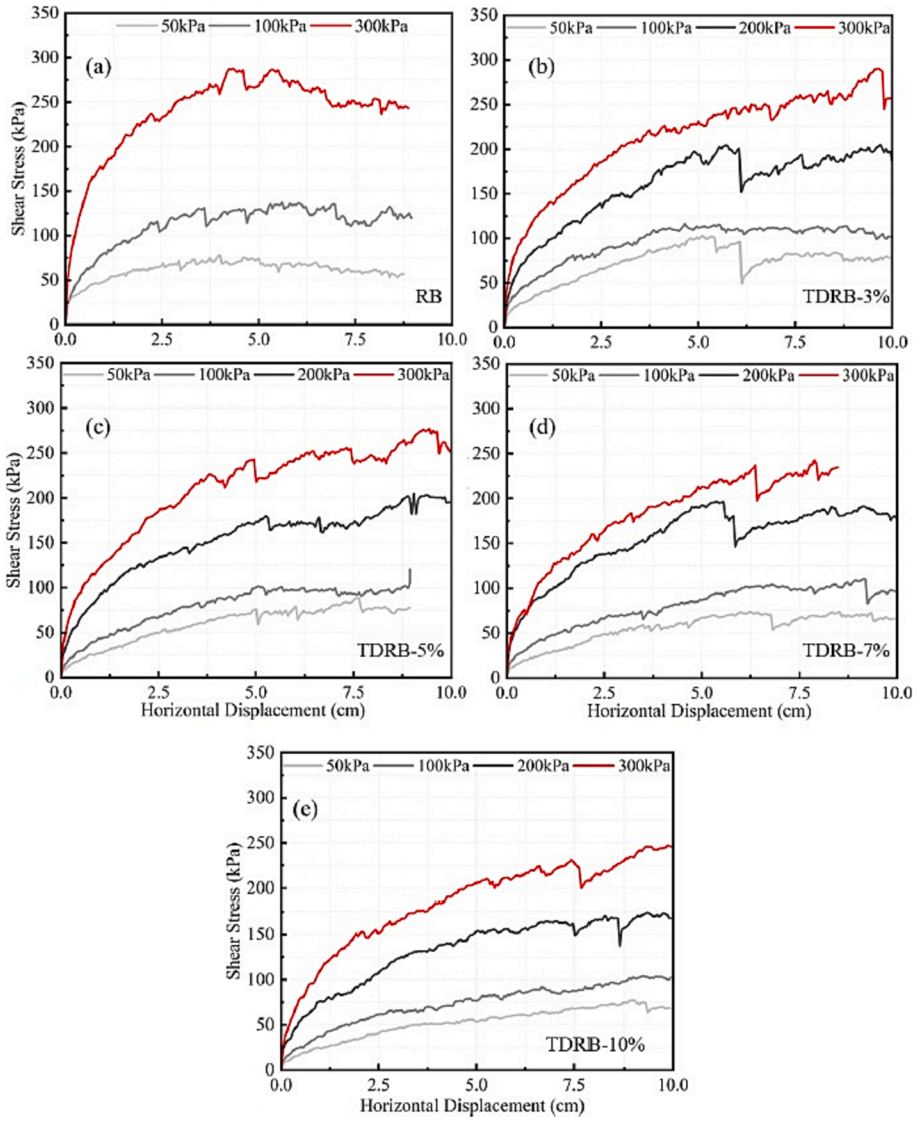

Fig. 5. Shear stress vs horizontal displacement curves from the direct shear test for samples a) RB (b) TDRB-3% (c) TDRB-5% (d) TDRB-7% (e) TDRB-10%.

trains generating greater stress levels. Moreover, Indraratna et al. [77] reported that maximum cyclic vertical stresses in an experimental track section reached 230 kPa, with a peak of 415 kPa due to a wheel flat. This finding highlights that wheel defects can significantly increase stress levels, leading to accelerated ballast degradation. In this study, cyclic shear tests were conducted with normal loads of 50, 200, and 300 kPa, which represent the range of typical railway loads. During the strain-controlled simple shear tests, shear stress was measured as a function of varying strain. The tests were performed at lower loading speeds at low strain levels, which increased progressively with higher strains. The loading stages 1–10, as summarized in Table 4, present the shearing rate varied between 0.000125 mm/sec and 1.02 mm/sec and cyclic shear amplitude varied between 0.0019 mm and 15.32 mm, keeping a constant duration of 3 mins for each loading cycle. The testing program consisted of 15 simple shear tests conducted on RB, TDRB-3 %, TDRB-5 %, TDRB-7 %, and TDRB-10 % to characterize the effects of vertical stress and cyclic shear strain on secant shear modulus and damping ratio. Railway ballast undergoes cumulative deformation due to repeated train loads. This includes elastic, plastic, and breakage-induced deformation, with shear stiffness gradually decreasing as shear strains increase. Previously, McCartney et al. [49] conducted large-scale simple shear tests for cyclic shear strain amplitudes ranging from 0.1 % to 10 %, revealing a less significant change in the secant shear modulus beyond 3 % shear strain. For instance, in the TDA sample tested at a normal load of 76.6 kPa, the secant shear modulus at 0.1 % strain was 2400 kPa. This value decreased to 560 kPa at 3 % strain, and at 10 % strain, the shear modulus was measured at 420 kPa. This indicates that the decrease in shear modulus becomes less significant beyond the 3 % strain level. Hence, this study was conducted for ten loading stages with cyclic shear strain amplitudes ranging from 0.0005 % to 4 %. The constant frequency at all loading stages aimed to capture the material's quasi-static behavior at all strains due to cyclic loading, ensuring the reproducibility and comparability of results. The gradual increase of amplitude at each stage of the test was expected to simulate the different levels of ballast deformation under cyclic shear loading. Further, with the increase of amplitude, the loading rate was also increased in each stage to mimic different shear force levels exerted by the train movements. This approach was adopted to characterize the non-linear elastic behavior of ballast observed under cyclic loading, particularly at high strain levels. It provides practical insights into ballast performance by quickly assessing stiffness and energy absorption. As shown in Figs. 3 and 4(b), load cell-1 was used to measure the applied constant normal load, and load cell-2 was used to measure the shear load generated due to the applied cyclic shear of the specimen. Further, two horizontal transducers were fixed at positions x1 and x2 with a vertical spacing h, representing the relative displacement measurements at the top and

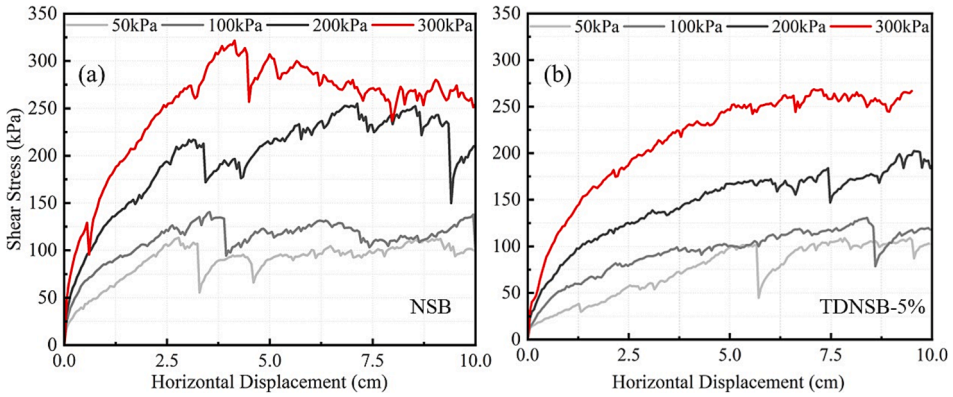

Fig. 6. Shear stress vs horizontal displacement curves from the direct shear test for samples (a) NSB (b) TDNSB-5%.

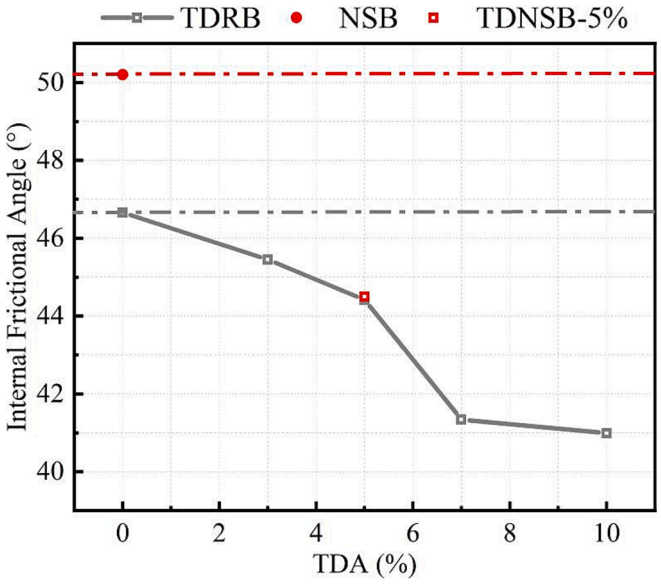

Fig. 7. (a) Variation of internal friction angle with TDA (%) addition.

bottom, respectively, as illustrated in Figs. 3 and 4(b). Accordingly, the corresponding shear strains from the applied cyclic shearing were calculated using Eq. (1).

$$\gamma = \frac{(\Delta x_2 - \Delta x_1)}{h} \quad (1)$$

where Δx_2 and Δx_1, represent the relative displacements between the base and at the top, and h is the vertical spacing. As shown in Fig. 4(c)& (d), the RB and TDRB samples were prepared in a simple shear box, considering their respective densities. Fig. 4(e) displays the particle breakage and the accumulation of finer particles at the bottom following the cyclic simple shear tests. These degraded samples were subsequently used to evaluate the BB Index (BBI).

Results and discussion

Shear strength characteristics

This study presents the shear strength characteristics obtained from monotonic direct shear tests conducted on all TDRB mixtures, NSB and TDNSB-5 %. Fig. 5(a)-()–(e))–(depicts the curves illustrating the variations in shear stress (kPa) with horizontal displacement for the RB and TDRB mixtures. The stress-displacement curves indicate that the TDRB mixtures exhibit a lower peak shear stress at each normal loading stage compared to the RB sample. This was due to the TDAs in the TDRB mixtures acting as a flexible, low-friction filler, reducing the direct contact and friction between gravel particles. Consequently, this reduces the TDRB material's shear resistance, leading to a lower peak shear stress under the same normal stresses compared to the RB sample. Moreover, materials undergo significant elastic and plastic deformation, reorganization, and breakage at higher displacements. Fig. 6(a)&(b) illustrates the comparisons of stress-displacement curves for RB, NSB, and TDNSB-5 %. The peak stresses of NSB were found to be higher than that of RB because the NSB materials were newly sourced, possessing good angularity and greater frictional resistance between the granular particles. Further, the results presented in Fig. 5(a)-()–(e))–(and Fig. 6(a)& (b) clearly demonstrate that ballast breakage was caused by shearing, as evidenced by the sharp drops (stick–slip behavior) observed in the stress-displacement curves. The TDRB mixtures displayed stick–slip behavior with TDA content ranging from 0 to 7 %. The higher percentage of TDA, such as 10 %, displayed more stable curves, which suggests a reduction in stick–slip behavior and less abrupt stress releases. Sadeghi et al. [38] presented the stress-displacement curves for

Table 5
Friction angle comparison of ballast materials.

TDA Content	Friction angle					
	Present study	Present study	Song et al. (2019) [42,43]	Sadeghi et al. (2025) [34]	Sadeghi et al. (2025) [34]	Qi et al. (2024) [35]
(%)	Reused limestone ballast + TDA size 22.4–50 mm °	Fresh limestone ballast + TDA size 22.4–50 mm °	Fresh ballast (granite) + TDA size 8–63.5 mm °	Fresh ballast (igneous rock) + TDA size 30 mm °	Fresh Ballast (igneous rock) + TDA size 5 mm °	RIBS (triaxial tests) °
0	46.6	50.2	38.7	48.5	48.5	56
3	45.5	–	–	44 (TDA −2.5 %)	48.2 (TDA −2.5 %)	
5	44.5	44.5	34.6	43.3	48	54
7	41.4	–	–	38.4	45	
10	41	–	29.5	37 (TDA −7.5 %)	44 (TDA −7.5 %)	51.3
15	–	–	–	35.5 (TDA −12.5 %)	43 (TDA −12.5 %)	48.5

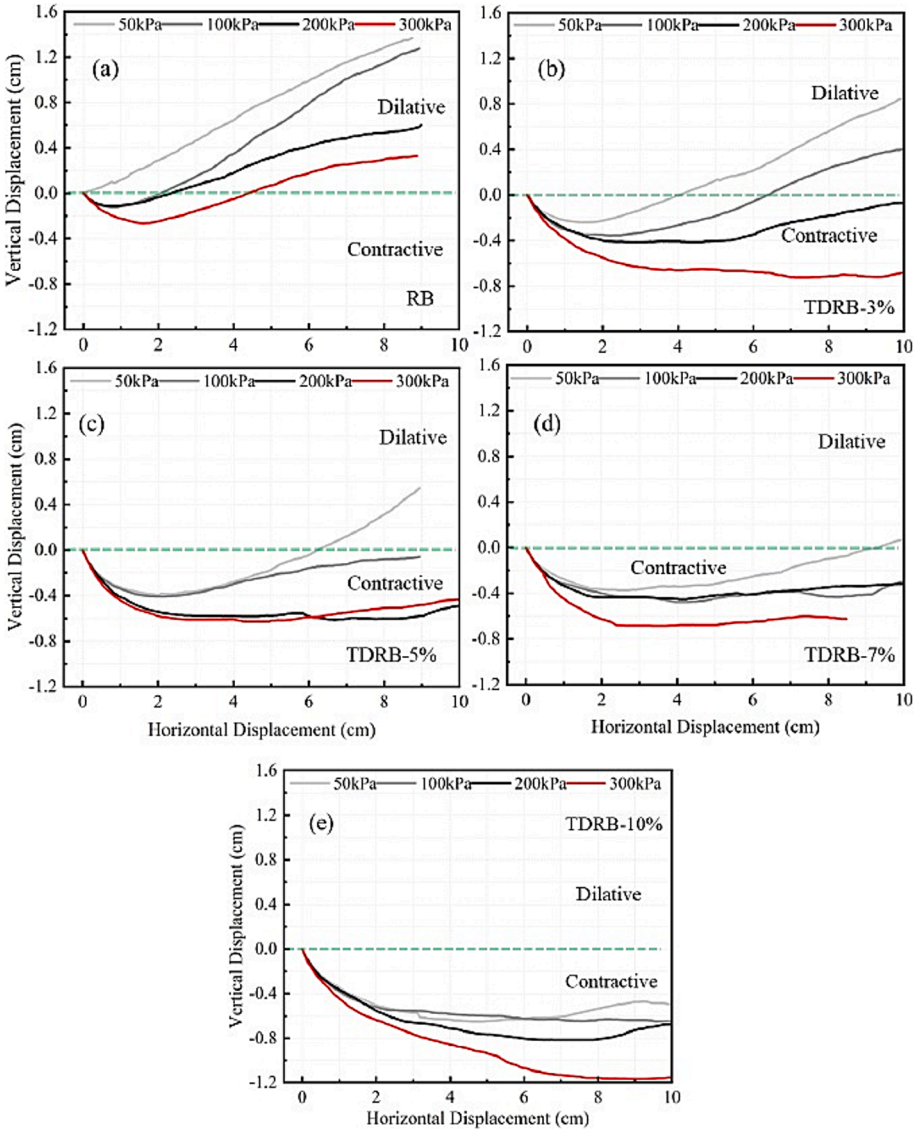

Fig. 8. Vertical displacement vs horizontal displacement curves from the direct shear test for samples (a) RB (b) TDRB-3% (c) TDRB-5% (d) TDRB-7% (e) TDRB-10%.

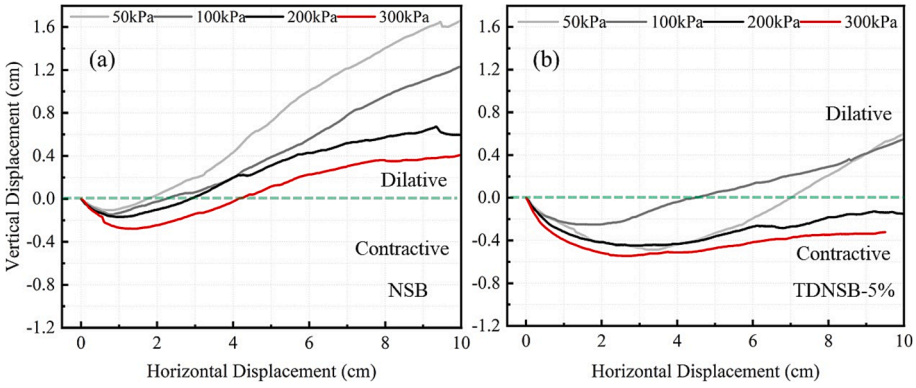

Fig. 9. Vertical displacement vs horizontal displacement curves from the direct shear test for samples (a) NSB (b) TDNSB-5%.

various ballast mixtures with TDA sizes varying from 1-30 mm, indicating a stick–slip behavior with large TDA particle sizes. Further, they asserted that larger TDAs behave more like ballast grains, experiencing and transmitting larger shear forces, leading to more pronounced stick–slip behavior. In contrast, smaller-sized TDAs are primarily utilized for filling voids rather than for a significant role in transmitting shear forces, which results in a more uniform stress distribution, thereby minimizing sudden force-slip events. Similarly, researchers [47,48] observed stick–slip behavior with the addition of 5 % TDAs with 8–63.5 mm size to the ballast mixtures. Further, the RB material in the present

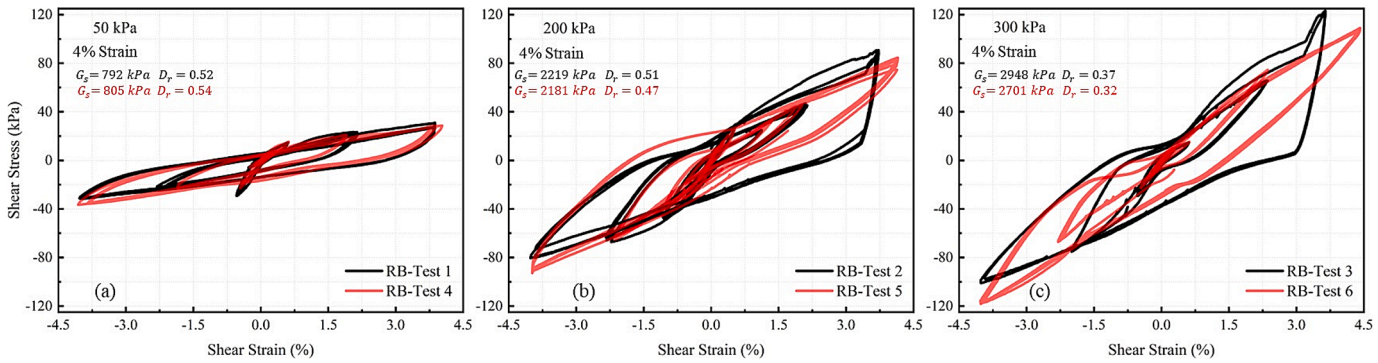

Fig. 10. Shear stress vs shear strain curves from the cyclic simple shear test for RB samples (a) RB at normal stress 50 kPa, (b) RB at normal stress 200 kPa, (c) RB at normal stress 300 kPa.

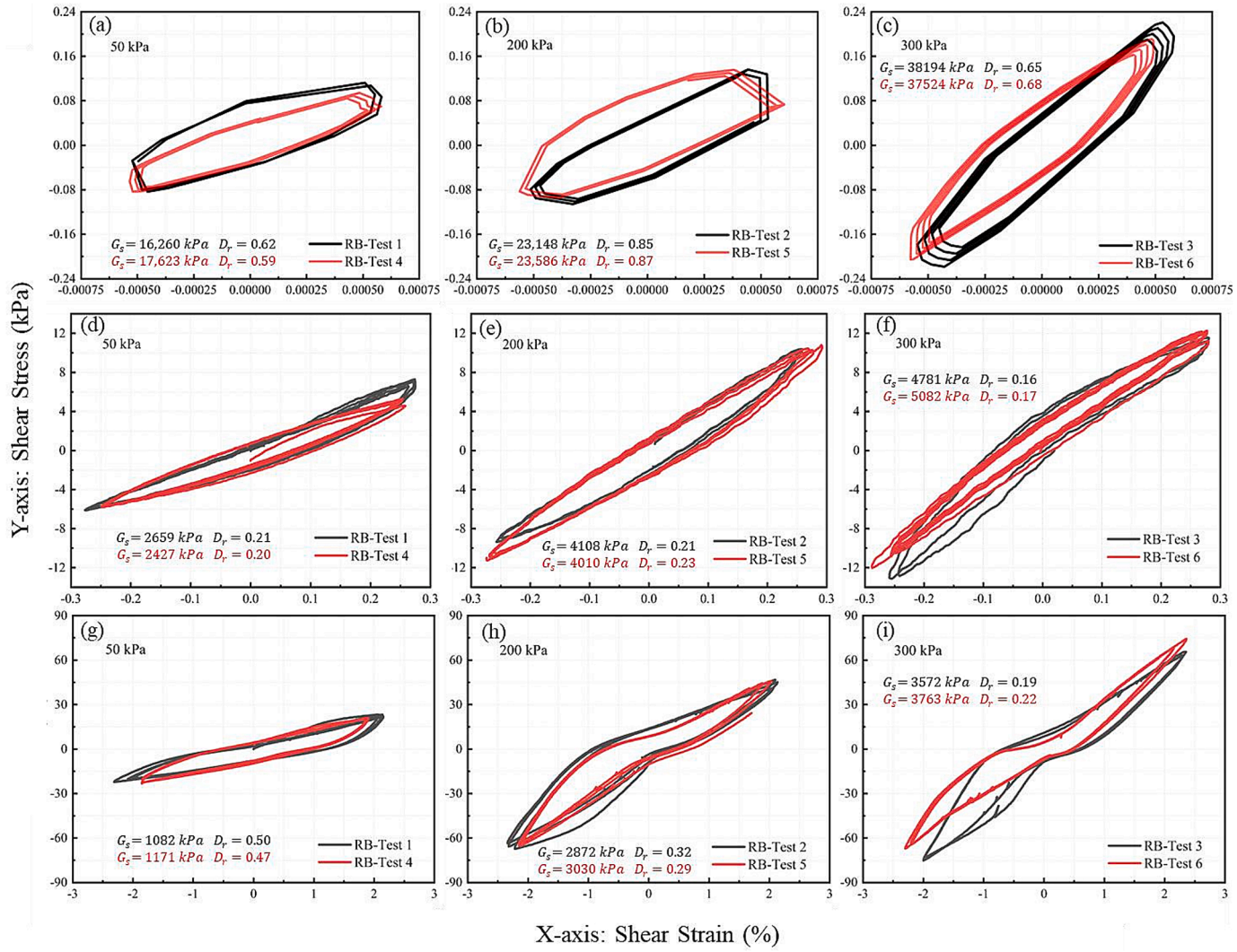

Fig. 11. Close-up view of shear stress vs shear strain curves of RB samples (a) RB at normal stress 50 kPa and 0.0005 % strain, (b) RB at normal stress 200 kPa and 0.0005 % strain (c) RB at normal stress 300 kPa and 0.0005 % strain (d) RB at normal stress 50 kPa and 0.25 % strain, (e) RB at normal stress 200 kPa and 0.25 % strain (f) RB at normal stress 300 kPa and 0.25 % strain (g) RB at normal stress 50 kPa and 2 % strain, (h) RB at normal stress 200 kPa and 2 % strain (i) RB at normal stress 300 kPa and 2 % strain.

study showed a reduced stick–slip behavior compared to TDRB, NSB, and TDNSB-5 %, which can be attributed to the degradation of the granular particles from previous use. The significant rounding and degradation of these particles decreased interlocking, leading to fewer abrupt stress drops. Moreover, the stick–slip behavior in NSB material arises from fresh particles with sharper edges and higher angularity, resulting in stronger interlocking and abrupt force redistributions. The particle gradation of TDAs, which range from 22.4 to 50 mm, was like those of reused ballast material. This implies that larger TDA particles significantly participate in the shear interlocking and transmitting the

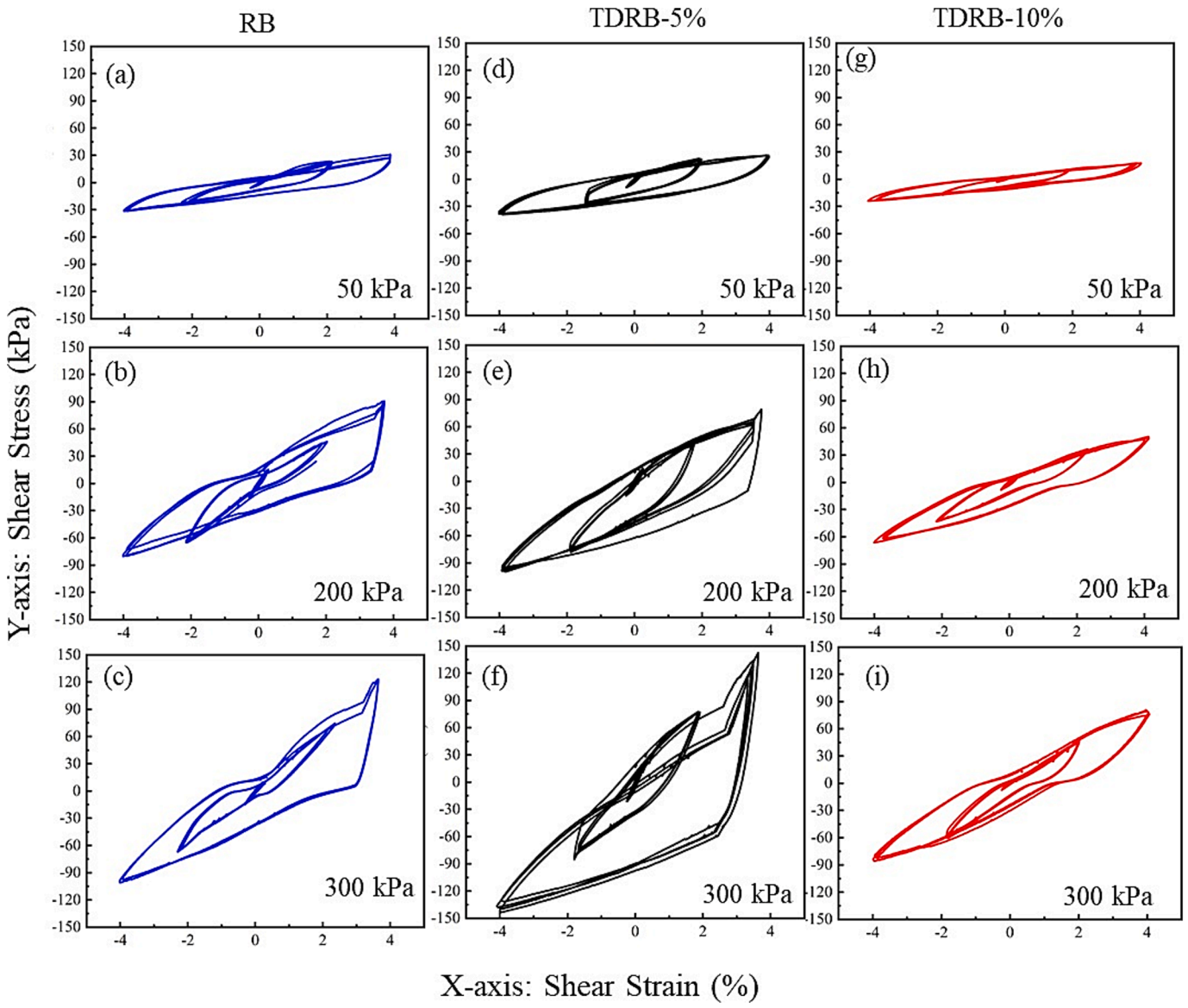

Fig. 12. Shear stress vs shear strain curves from the cyclic simple shear test for samples (a) RB at normal stress 50 kPa (b) RB at normal stress 200 kPa (c) RB at normal stress 300 kPa (d) TDRB-5 % at normal stress 50 kPa (e) TDRB-5 % at normal stress 200 kPa (f) TDRB-5 % at normal stress 300 kPa (g) TDRB-10 % at normal stress 50 kPa (h) TDRB-10 % at normal stress 200 kPa (i) TDRB-10 % at normal stress 300 kPa.

shear forces in the TDRB mixtures.

The internal friction angle for all tested samples was estimated from the obtained peak shear stresses and the applied normal stresses using the Mohr-Coulomb failure criterion. Fig. 7 shows the internal friction angle results for TDRB and TDNSB mixtures with different TDA contents. The friction angle for RB, without any TDA content, was observed to be $\varphi = 46.6^{\circ}$. The internal friction angle (φ) decreased from 46.6° to 41° with an increase in TDA content from 0 % to 10. In the case of TDRB-5 %, the friction angle was around 44.5°, which was not a significant decrease. Meanwhile, the friction angle for NSB without TDA content was 50.2°, higher than that of the RB sample. Table 5 presents the internal friction angle comparisons of various TDA mix ballast materials obtained from the current and previous studies. The comparison shows that adding TDA to RB mixtures had a minimal effect on friction angle compared to TDNSB mixtures. Notably, the friction angles for TDRB-5 % and TDNSB-5 % were identical, highlighting a more pronounced friction-angle reduction in TDNSB-5 % relative to NSB. This observation aligns with findings by Song et al. [47,48] and Sadeghi et al., [38], who reported a substantial decrease in friction angles (from 38.7° to 34.6° and from 48.5° to 43.3°, respectively) with the addition of 5 % TDA compared to fresh ballast. These findings suggest that incorporating TDAs has a more pronounced effect on lowering the friction angle of TDNSB compared to TDRB mixtures.

Fig. 8(a)–(e) presents the horizontal and vertical displacement variations of the RB sample and TDRB mixtures. The dilatancy and contractive behavior from these curves were interpreted based on the vertical displacement: dilatancy is shown by a positive vertical displacement, reflecting the upward movement of the samples, whereas negative displacement values indicate sample contraction. Fig. 8(a) shows that the RB sample demonstrated dilatant behavior across all normal loads. Initially, contractive behavior was observed under higher normal stress; however, the RB samples displayed dilative behavior as shear progressed. This observation aligns with findings reported by Indraratna et al., [77] indicating similar dilatant behavior in large-scale triaxial tests conducted on railway ballast. Additionally, they noted that dilation, or volumetric increase, occurs in ballast specimens subjected to monotonic loads at various confining pressures. The TDRB mixtures, on the other hand, displayed both dilatant and contractive behavior

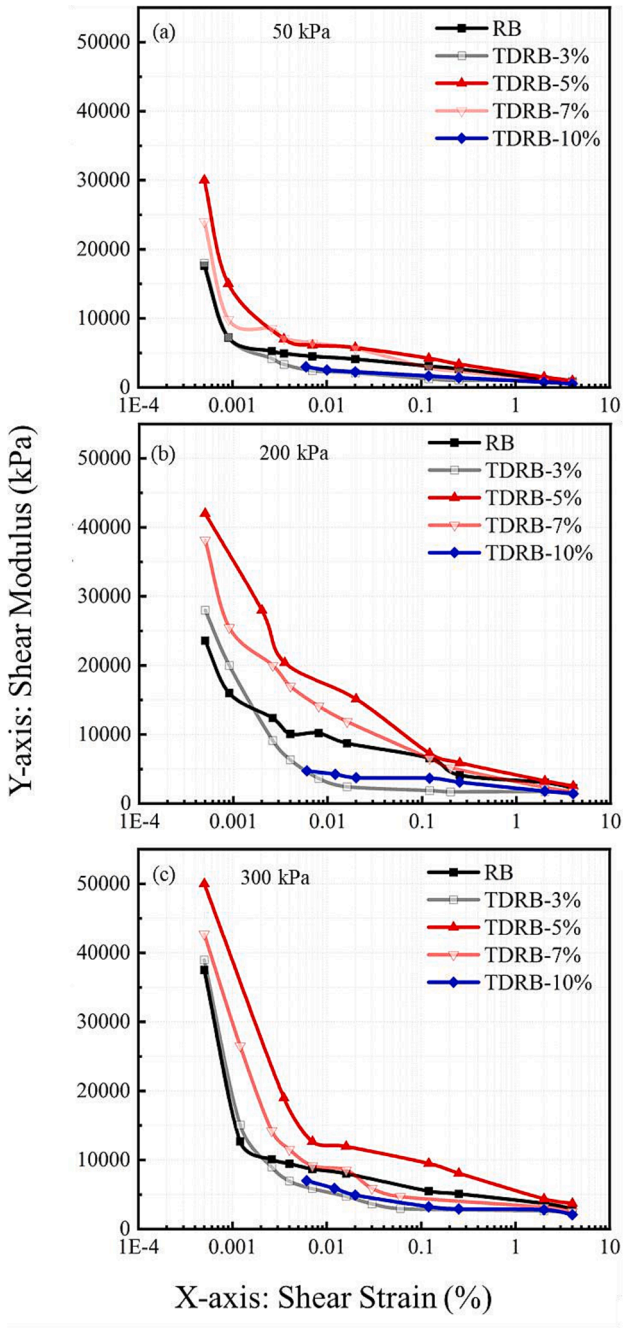

Fig. 13. Variation of shear modulus with shear strain at normal stress (a) 50 kPa (b) 200 kPa (c) 300 kPa.

depending on the applied normal stresses. As shown in Fig. 8(b), the TDRB-3 % sample exhibited dilatant behavior under normal stresses of 50 kPa and 100 kPa. However, at higher normal stresses of 200 kPa and 300 kPa, the negative vertical displacement values indicated contractive behavior. Likewise, with increasing TDA content, the TDRB samples transitioned from dilatant to contractive behavior, as presented in Fig. 8 (c)&(d). Researchers [47,48] made similar observations, indicating that as normal stress increased from 50 kPa to 150 kPa, the behavior of the TDA mixed ballast material changed from dilation to compression. Moreover, with 10 % TDA content, contractive behavior was observed across all applied normal stresses, as shown in Fig. 8(e). This indicates that the higher TDA content significantly influenced the mechanical behavior of the TDRB mixture, allowing the material to compress more readily under shear instead of dilating. As observed, the reduction in the frictional angle of TDRB mixtures indicates that the presence of TDAs decreases the frictional resistance between particles. Consequently, there is reduced inter-particle movement or sliding, which usually causes dilatancy. The mixture starts to behave less like a dense, interlocked granular material and more like a compressible matrix, with TDAs cushioning the gravel particles. The TDAs deform and absorb part of the shear stress, decreasing the material's overall tendency to expand. Therefore, as TDA content increases, the TDRB mixture exhibits characteristics like a composite material with greater compressibility. Furthermore, Fig. 9(a)&(b) illustrate the horizontal and vertical displacement variation curves for the RB, NSB, and TDNSB-5 % samples. The results indicate that NSB showed higher dilatancy than the RB sample, which is expected given that NSB is a newly sourced material. This behavior can be corroborated by its increased shear strength characteristics. However, with the addition of 5 % TDA to NSB, a change from dilatant to contractive behavior was observed, akin to the TDRB mixtures.

Cyclic simple shear test results

Cyclic simple shear tests were conducted on RB and TDRB mixtures under constant normal loads of 50, 200, and 300 kPa. These large-scale experiments were focused on determining the secant shear modulus and damping ratio variations under cyclic loading conditions. Under strain-controlled conditions, shear stresses were measured, and cyclic loading was applied to generate cyclic shear hysteresis curves.

To evaluate repeatability and reliability of the large-scale cyclic simple shear test methodology, two sets of tests were initially conducted on reused ballast (RB) material under three normal stresses: 50 kPa (RB-Test 1 & 4), 200 kPa (RB-Test 2 & 5), and 300 kPa (RB-Test 3 & 6). All tests (RB-Test 1 through 6) were performed under strictly controlled sample preparation and identical loading conditions to ensure procedural consistency. Fig. 10(a)-()–(c))–(present the cyclic stress–strain curves from repeated tests. The results demonstrate a high degree of consistency between the paired tests, with closely matching shear modulus and damping ratio at 4 % strain, confirming the accuracy and repeatability of the testing approach. However, minor deviations in stress–strain curves observed at larger strain levels indicate potential particle rearrangement, leading to variations in shear resistance without proportional changes in shear strain – an effect more pronounced under higher normal stresses.

Additionally, Fig. 11(a)–(f) display stress–strain responses at selected strain levels – 0.0005 %, 0.25 %, and 2 %, representing low, intermediate, and high strain ranges, respectively. The strong agreement across repeated tests and strain levels confirms the robustness of the test setup and validates its applicability for characterizing the behavior of all TDRB mixtures.

The cyclic shear stress–strain relationships for RB, TDRB-5 %, and TDRB-10 % are depicted in Fig. 12(a)-()–(i))–(, showing differences in hysteretic loops during cyclic shear loading, both with and without TDA content. Fig. 12(a)-()–(c))–(highlights the cyclic stress–strain curves for RB samples tested at strain levels from 0.0005 % to 4 % under normal loads of 50 kPa, 200 kPa, and 300 kPa. The peak shear stresses observed at 4 % strain were lower compared to those of TDRB-5 % at normal loads of 200 kPa and 300 kPa. In addition, Fig. 12(d)-()–(f))–(displays a larger area under the curves at each strain level for TDRB-5 %, reflecting higher energy dissipation due to the 5 % TDA content. However, with a further increase in TDA content to 10 %, peak shear stresses and energy dissipation were reduced, as shown in Fig. 12(g)-()–(i))–(. Further, at a normal stress of 50 kPa, these figures indicate that the hysteresis loops are symmetric about the origin for RB, TDRB-5 %, and TDRB-10 %. According to McCartney et al. [49], the relationship between shear strain and stress exhibits nonlinearity and symmetry about the origin, like the hysteresis loops observed in this study. For TDA-100 %, they reported a peak shear stress of 18 kPa at 4 % shear strain under a normal stress of 57 kPa. In comparison, in the current study, peak shear stress

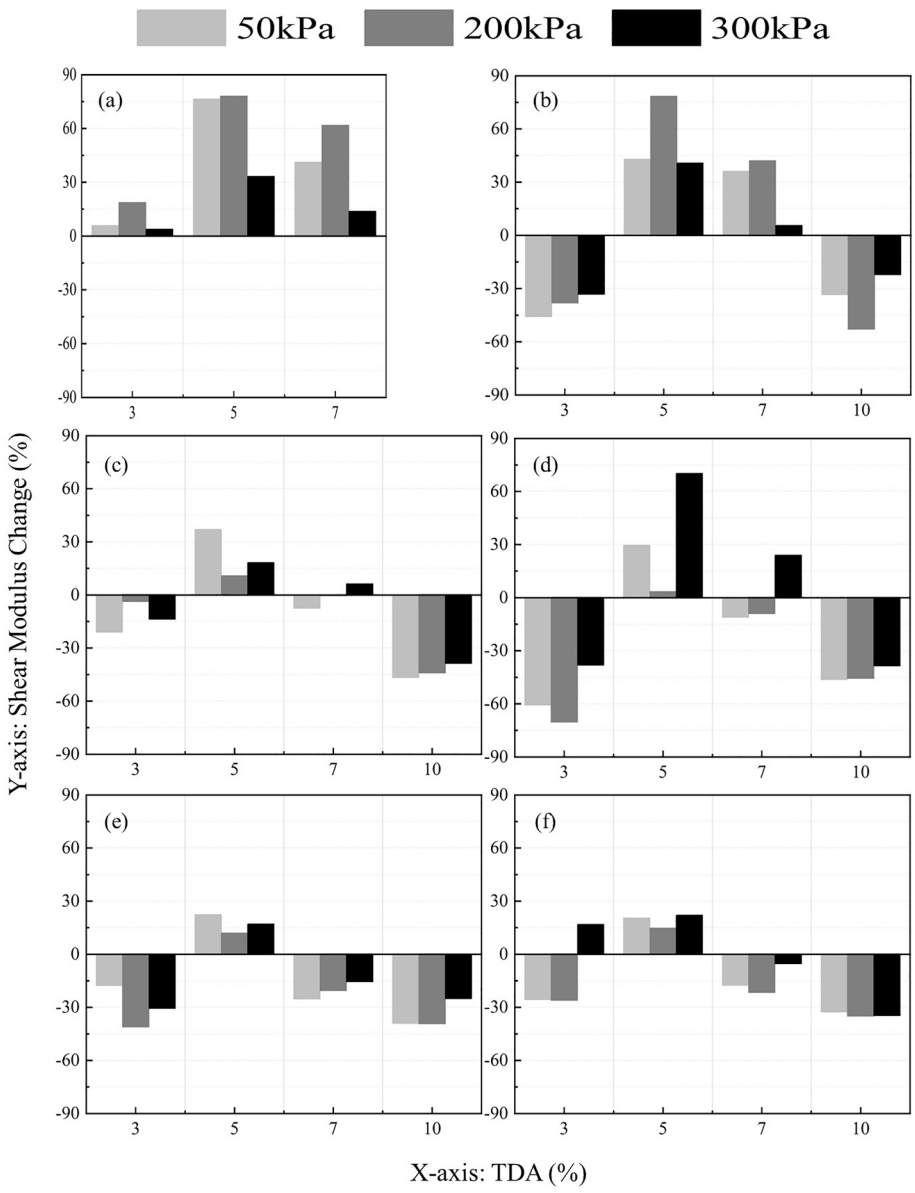

Fig. 14. Percentage change in shear modulus with TDA% at Strain level (a) 0.0005 % (b) 0.004 % c) 0.12 % d) 0.25 % e) 2 % f) = 4 %.

values at 4 % shear strain for RB, TDRB-5 %, and TDRB-10 % were 35 kPa, 38 kPa, and 24 kPa, respectively at a normal stress of 50 kPa. Further, in the present study, a sharp drop in stress at 4 % strain limits for TDRB-5 % was observed, like RB samples, at normal stresses 200 kPa and 300 kPa. However, this behavior was not exhibited in TDRB-10 % samples. This behavior can be corroborated with the stress-displacement curves in Fig. 5 (e) TDRB-10 %, where no significant stick–slip effects were observed. Adding 10 % TDAs by mass significantly increased the volume within the simple shear box, where the particle size was like ballast. These findings suggest that TDRB-5 % provides an optimal balance between ballast interlocking and rubber flexibility, whereas TDRB-10 % behaves more similarly to the 100 % TDA reported by McCartney et al. [49], reducing interparticle friction.

Shear modulus variation

The results were further analyzed to explore the relationship between shear modulus with shear strain. The shear modulus was calculated as the ratio of the difference in maximum and minimum shear stresses to the corresponding difference in shear strains at each strain level. Fig. 13(a)-()–(c))–(shows the variation in shear modulus with shear strain for different sample configurations, indicating that TDRB-5 % had a higher shear modulus across all applied normal loads. Song et al. [47] reported that the interface shear stiffness obtained from cyclic direct shear tests decreased with the addition of TDA content in fresh ballast material. However, in the present study, the shear modulus of RB was found to be lower compared to TDRB-5 % and, in some cases, like shear modulus of TDRB-3 % and TDRB-7 %. To better understand these differences, the percentage change in shear modulus values for various TDRB mixtures with different TDA contents was calculated in relation to the base value of the RB samples, as described in Eq. (2).

$$\%\,\text{change in values} = \frac{V_{TDBM} - V_{BM}}{V_{BM}} \times 100 \tag{2}$$

where V_{TDBM} is the result value of the sample TDRB mixture, V_{BM} is the result value of the sample reused ballast material. The percentage change in shear modulus at shear strains of 0.0005 %, 0.005 %, and 4 % is depicted in Fig. 14(a)-()–(f))–(. The positive changes in values signify that the TDRB-5 % mixture performed better. However, monotonic direct shear tests showed that the peak shear stresses were higher for RB but decreased as the TDA content in TDRB mixtures increased. These

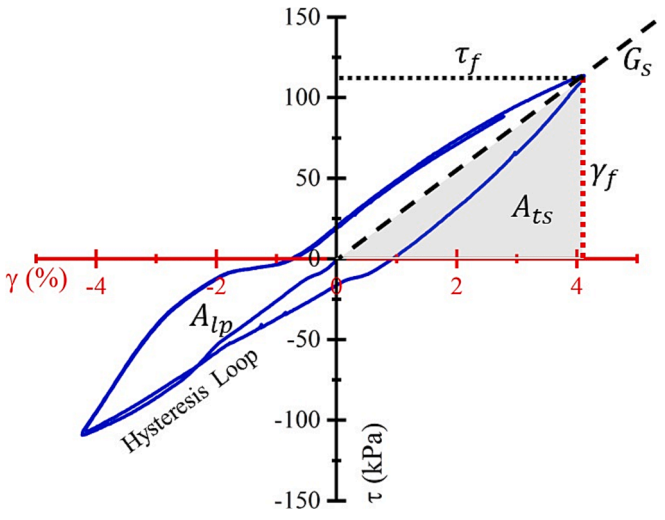

Fig. 15. Illustration of hysteresis loop for the evaluation of damping ratio (RB sample at shearing stage-10 and normal stress 300 kPa).

monotonic direct shear tests were strongly influenced by inter-particle friction and interlocking. With higher TDA content, the shear stress declines because of reduced inter-particle friction and greater cushioning. On the other hand, the cyclic simple shear test involves repeated loading and unloading cycles that simulate quasi-static conditions. In this test, the shear modulus reflects the material's stiffness and its ability to recover or resist deformation under repeated shear loads, which is not the same as the shear stresses measured in the direct shear test. Further, at 10 % TDA content, the mixture may become more heterogeneous. The distribution of TDA could create pockets or zones within the material that behave differently under cyclic shear, leading to a more inconsistent and generally lower shear modulus. This variability in stiffness could be due to differences in local concentrations of TDA, creating softer regions that reduce the overall modulus. The initial increase in shear modulus at 5 % rubber content suggests an optimal balance where the benefits of TDA (like energy absorption and slight cushioning) enhance the TDRB's overall performance. However, as the TDA content continues to increase, these benefits reduce due to the increase in the volume occupied by these TDAs.

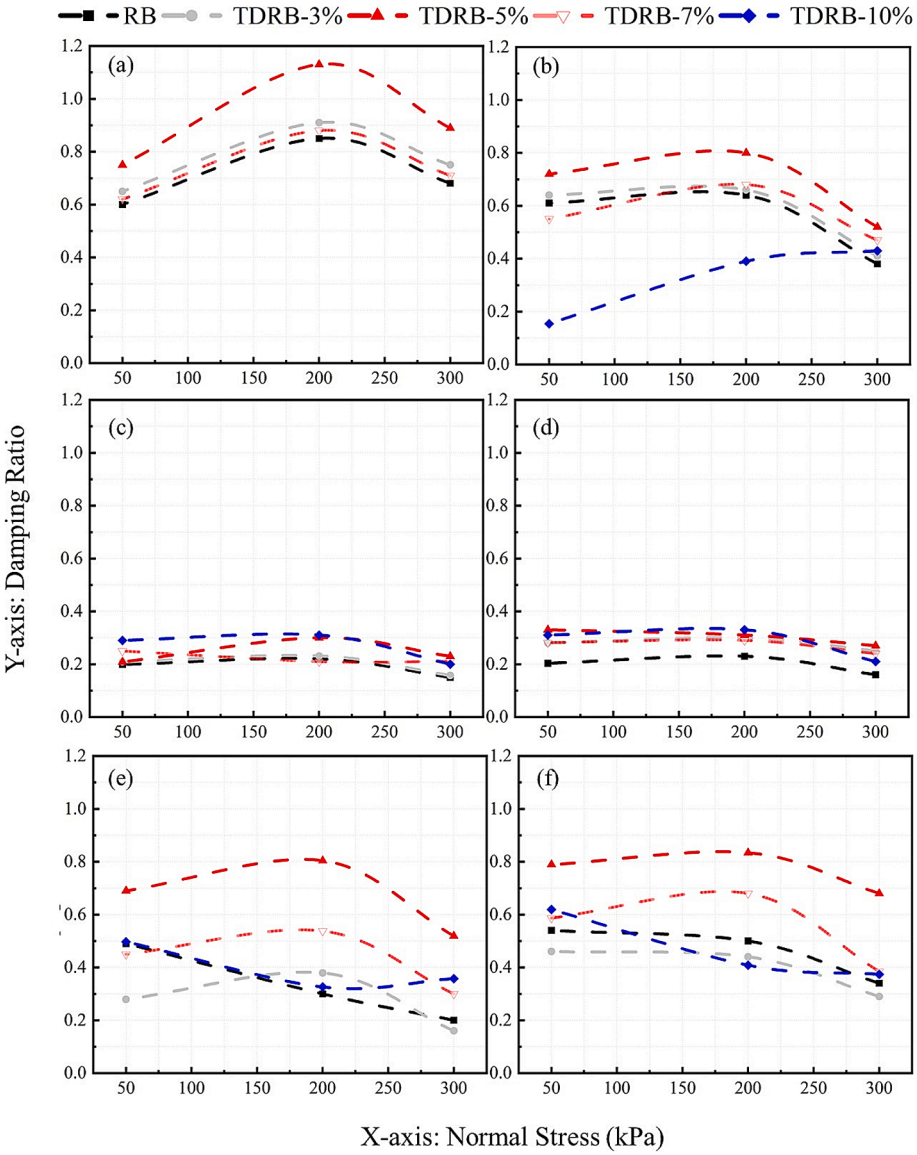

Fig. 16. Variation of damping ratio with normal stress at strain level (a) 0.0005% (b) 0.004% c) 0.12% d) 0.25% e) 2% f) 4%.

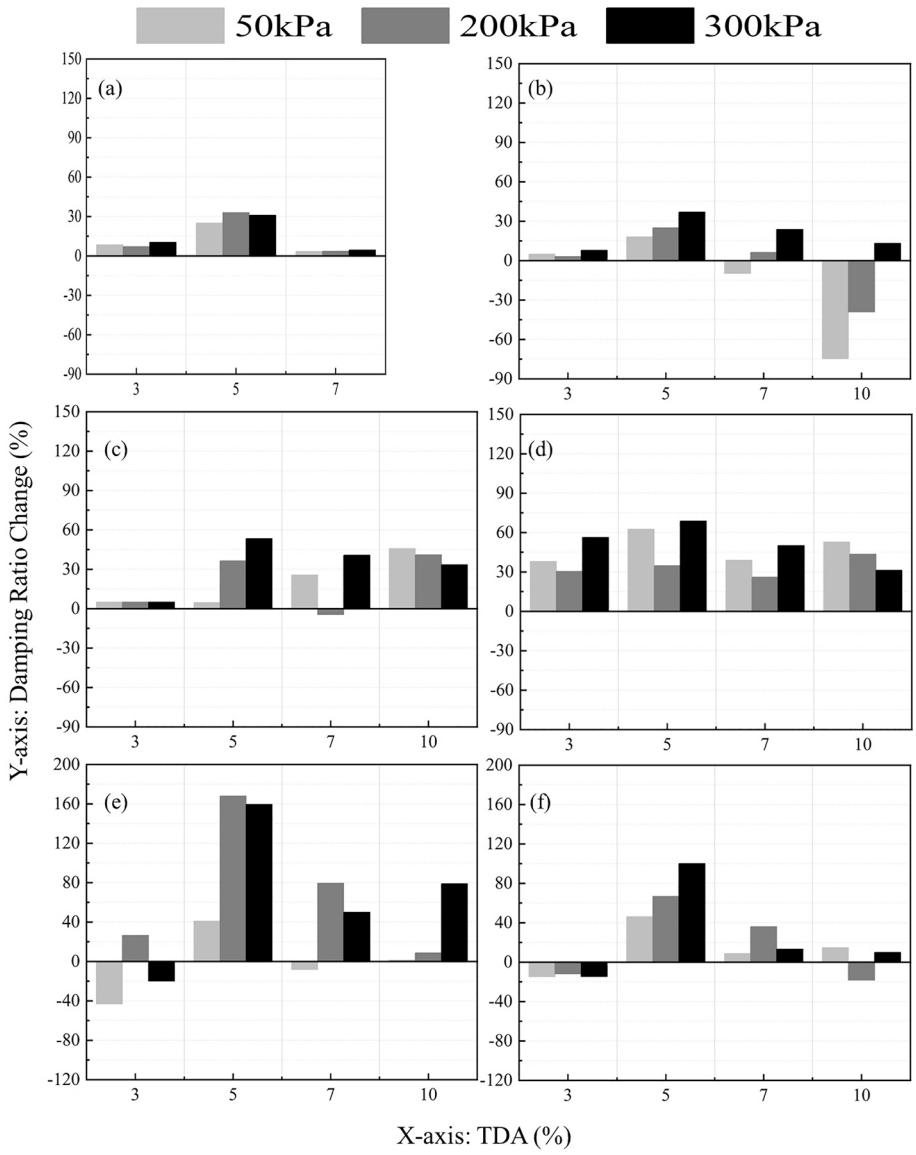

Fig. 17. Percentage change in damping ratio with TDA% at (a) 0.0005% (b) 0.004% c) 0.12% d) 0.25% e) 2% f) 4%.

Damping ratio variation

The damping ratio at each strain level was calculated from the hysteresis damping curves, as shown in Fig. 15, defined as the ratio of energy loss to energy input per cycle, according to Eq. (3).

$$D_r = \frac{A_{lp}}{4\pi A_{ts}} \tag{3}$$

where D_r is the damping ratio, A_{lp} is the area hysteric loop representing energy dissipation, A_{ts} is the area of the triangle formed by the peak shear stress, and shear strain at each strain level, τ_f and γ_f are the shear stress (kPa) and shear strain (%) at respective cyclic strain levels, and G_s is the secant shear modulus (kPa). Fig. 16(a)-()–(f))–(present the damping ratios for each sample at various shear strain levels. The evaluated damping ratio was high at low strains, decreased at intermediate strains, and increased again at higher strains. The RB and TDRB mixtures at lower strains experience smaller deformations, primarily dissipating energy through inter-particle friction and subtle particle rearrangement. The enhanced damping in the TDRB mixtures was due to micro-scale interactions, where particles can move, slide, and dissipate energy efficiently. As strain rises, these mixtures begin to enter a non-linear deformation regime. In this phase, the particles become more tightly packed, restricting their ability to move or slide freely. Consequently, energy dissipation decreased, and the material showed a stiffer response. The stiffening at intermediate strains reduces inter-particle sliding, resulting in a lower damping ratio. After this, the system transitioned into a non-linear elastic regime, where increased particle movement at higher strains facilitated more efficient energy dissipation. McCartney et al. [49] reported similar findings, noting higher damping ratios at low strains, a decrease at intermediate strains, and an increase at high strains in cyclic simple shear tests of 100 % TDA. Furthermore, these results are consistent with one of Feng and Sutterer's [78] tests on granulated rubber. TDAs function as a soft buffer, enhancing energy dissipation by allowing small particle movements and deformations within the ballast. At higher strains, the TDA's flexibility permits greater deformation while the ballast maintains structural integrity. This results in improved energy absorption and a higher damping ratio. TDRB-5 % was found to be the optimal ballast mixture for energy dissipation, while 3 % TDA content was insufficient to affect the material's damping properties. Researchers [35,36], based on cyclic triaxial tests, observed that the damping ratio varied from 0.7 to 0.3 as the TDA content (with particle sizes of 9–13.5 mm) decreased from 15 % to 0 % in ballast material under an effective confining pressure of 60 kPa. However, in the present study, at higher percentages (such as 7 % and 10 %), the

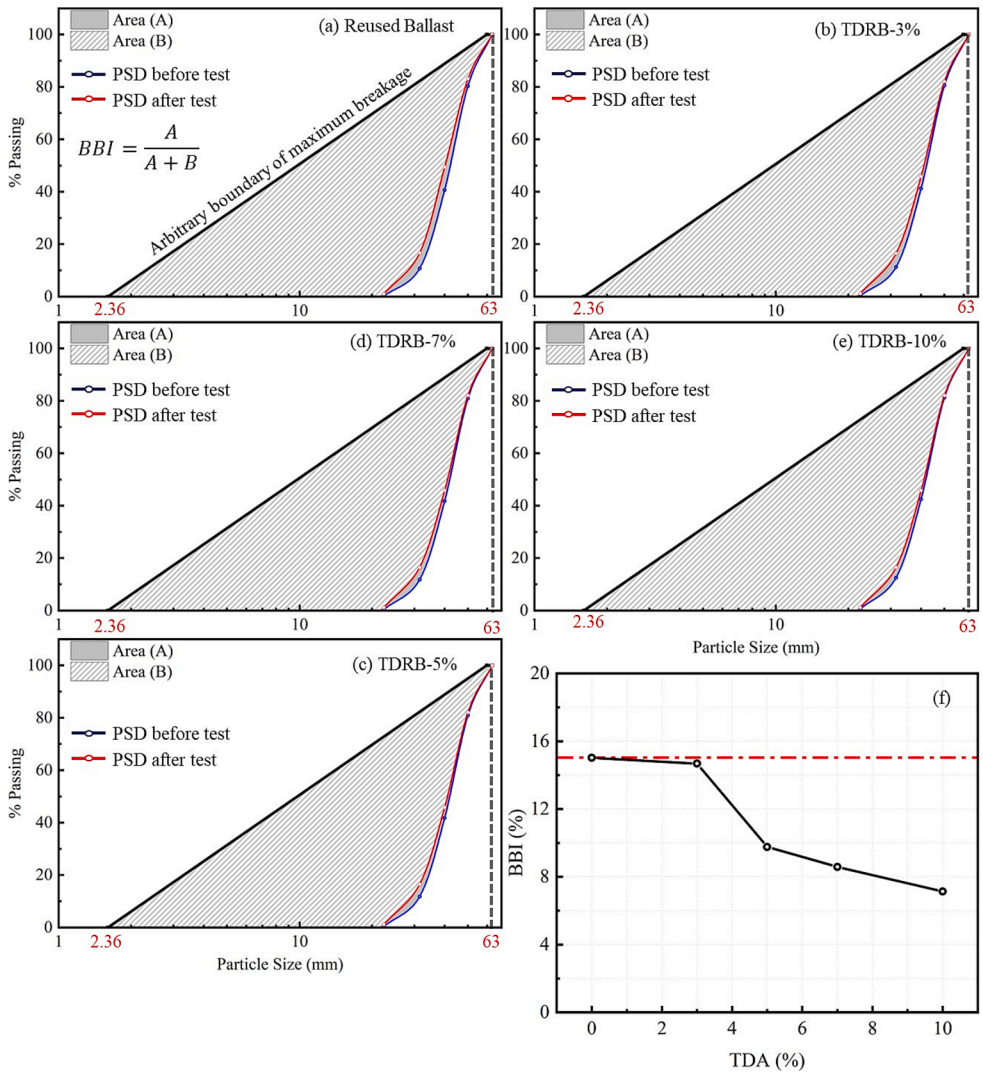

Fig. 18. Ballast Breakage Index a) RB (b) TDRB-3% (c) TDRB-5% (d) TDRB-7% (e) TDRB-10% (f) BBI variation with TDA (%) addition.

TDAs with larger particle sizes (22.4–50 mm) start to dominate, softening the composite and decreasing its stiffness. In addition, energy dissipation at higher TDA content declined as the formation of individual pockets reduced the energy absorption from large cyclic deformations effectively.

Fig. 17(a)–(f) shows the percentage change in the damping ratio at shear strains of 0.005 % and 4 %. The enhanced damping and shear modulus in the TDRB-5 % mixture indicate that using an optimal 5 % TDA content improves the performance of the modified ballast material. According to Esmaeili et al. [51], tests on the damping ratios of ballast materials yielded different outcomes from the shear tests. Their cyclic uniaxial tests revealed that ballast with 5 % TDA exhibited the lowest damping ratio of 0.098, while the damping ratios for ballast with 0 % and 10 % TDA were 0.202 and 0.434, respectively. These results indicate that incorporating TDA tends to increase the damping ratio of ballast. However, in the present study, it was observed that beyond 5 %, TDA content with larger particle size (22.4–50 mm) did not contribute further to energy dissipation or load transfer; instead, it started to undermine the granular structure of the ballast, reducing both shear modulus and damping.

Ballast breakage under cyclic shear loads

Several breakage indices have been developed to evaluate ballast breakage after monotonic and cyclic tests of ballast material [31,38,79]. This study used the ballast breakage index (BBI) defined by [53] to assess the ballast breakage under cyclic shear tests. The results of the monotonic direct shear tests, as illustrated in Figs. 5 and 6, clearly demonstrate that ballast breakage occurs during the shearing process, evident from the sharp drops in stress–strain curves. Furthermore, it is noteworthy that the extent of particle breakage is generally more pronounced in direct shear tests, as the samples are subjected to higher displacements or pushed to failure. Hence, this study evaluated the ballast breakage index (BBI) after the cyclic simple shear tests, representing the long-term behavior of ballast material with strains limited to 4 %. The estimation of the BBI for the samples is presented in Fig. 18(a). This figure depicts the particle size distribution (PSD) for the samples prior to testing, as well as the PSD for the degraded samples following the cyclic shear test conducted at a normal load of 300 kPa. The arbitrary boundary line of maximum breakage was used to quantify the area between the curves, and accordingly, the BBI was estimated according to the equation provided in Fig. 18(a). Each set of data was evaluated individually to facilitate a comprehensive analysis of the effects of TDA content on the BBI of the TDRB mixtures. The presented results indicate that the area between the PSD curves before and after the test decreased as the TDA content increased, as shown in Fig. 18(a)-()–(e))–(. This showed a decrease in the ballast degradation with the increase in TDA content from 3-10 %, which led to a decrease in the BBI for the TDRB

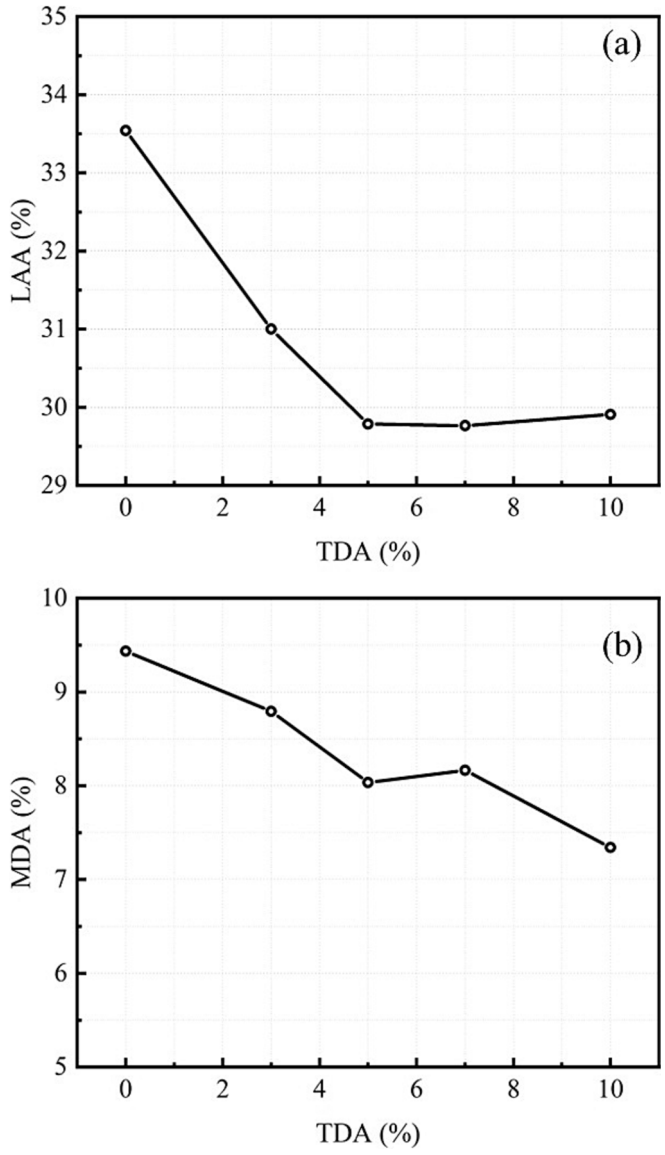

Fig. 19. (a) LAA variation with different TDA% (b) MDA variation with different TDA%.

mixtures. Fig. 18(f) illustrates the effect of TDA content on the BBI, demonstrating a decline from 15 % to 7.5 % as the TDA content increases from 0 % to 10 %. Notably, increasing the TDA content up to 5 % leads to a substantial reduction in BBI (from 15 % in RB to 9.75 % in TDRB-5 %). However, beyond a 5 % concentration, the changes in ballast behavior are minimal, as indicated by BBI values of 8.5 % for TDRB-7 % and 7.5 % for TDRB-10 %. Indraratna et al., [35] noted that at a 5 % TDA content with particle sizes ranging from 9.5 to 19.5 mm, the rubber particles functioned as void fillers, which helped to reduce ballast abrasion and breakage. The TDA particle size in the current study was larger (ranging from 22.4 to 50 mm), allowing the rubber aggregates to serve as a protective shield between the ballast particles, thereby minimizing interparticle abrasion. This action causes a noticeable decrease in ballast breakage at 5 % TDA content. However, increasing the TDA content further does not substantially decrease the BBI, as the formation of isolated TDA and granular pockets limits the TDA's impact on interparticle breakage. Sadeghi et al. [38] observed a similar trend, where using larger TDA particles (30 mm) effectively minimized particle breakage during cyclic direct shear tests. Furthermore, they found that a lower content of TDA with larger particle size increased the BBI compared to fresh ballast material. Additionally, they observed that smaller TDA particles resulted in increased particle segregation at the bottom due to cyclic loading. Summarizing the BBI observations from the present study, incorporating larger TDA particles at an optimal 5 % content helps mitigate forces that would otherwise cause ballast breakage at higher strains. This enhances the structural integrity of the ballast while still ensuring effective energy dissipation.

Ballast material degradation

The degradation of RB and TDRB ballast mixtures was assessed through LAA and MDA tests, with results compared to understand the effect of TDA content. Several international railway standards have established limits for ballast degradation based on LAA tests. These include Germany (BS EN 13450: 8.7–23 %), the USA (AREMA: 25–40 %), Australia (AS 1141: 25 %), Canada (CN: 20–30 %), the UK (BS EN 13450: 20 %), and India (IRS-GE-1: 30–35 %) [26]. These standards indicate that the maximum allowable LAA value for rail tracks with regular passenger and freight transport is 40 %, depending on the ballast class or rock source. Additionally, some standards specify limits for MDA tests, such as the UK (BS EN 13450: 7 %) and Iran (IR 301: 10–14 %). Fig. 19(a) shows that the LAA value of RB was 33 %, attributed to the limestone, a ballast rock material prone to higher degradation [69]. Guo et al. [26] observed that larger ballast particles generally have higher LAA values, lower wear resistance, and increased shear strength. Notably, adding TDA reduced LAA values below 30 %; however, increasing TDA content beyond 5 % had no significant impact. This can be attributed to a similar phenomenon observed in ballast breakage, where higher TDA content leads to the formation of individual pockets, resulting in more significant localized crushing compared to TDRB-5 %. The effect of TDA content on material degradation in the MDA test, as shown in Fig. 19(b), indicates a decline in MDA values from 9.5 % to 7.25 % for RB and TDRB mixtures with 3–10 % TDA. Unlike LAA variations, MDA values exhibit a consistent decrease with increasing TDA content. This can be attributed to the reduced degradation of ballast particles in water, where the MDA test smoothened their surfaces while the LAA test induced crushing.

Conclusion

The study presents the improved performance of reused limestone-based ballast material mixed with TDAs as a potential alternative to freshly sourced limestone ballast materials, aiming to reduce their dependency on railway infrastructures. A series of large-scale shear tests were performed to evaluate the behavior of RB and TDRB mixtures compared to the newly sourced ballast. In addition, the study demonstrates the development of a novel large-cyclic simple shear apparatus to evaluate the shear modulus and damping ratio from the hysteresis behavior obtained from the cyclic shear for ballast materials. This innovative testing method provides a fresh perspective on evaluating the deformation properties of ballast material for potential railway applications. In addition, BBI, LAA and MDA tests were employed to evaluate the ballast material degradation. The key findings from this analysis are summarized below:

1. The RB material has shown lower shear strength than the NSB material. With the addition of TDA content, the friction angle of the TDRB mixtures was reduced. However, the reduction of friction angle for the TDRB-5 % (FA = 44.5°) mixture compared to RB (FA = 46.6°) material was 5 %, which was insignificant. TDAs have shown a more pronounced impact on reducing the internal friction angle of fresh ballast materials.
2. The increase in TDA content in TDRB mixtures to 10 % reduced friction angle, shear modulus, and damping ratio, indicating that higher TDA content with larger particle size may compromise the mechanical properties of the recycled ballast mixture.

3. The TDRB mixtures demonstrate a lower ballast breakage index and reduced abrasion losses compared to RB, indicating their potential to improve the durability and service life of railway tracks.
4. Adding 5 % TDA by mass to reused ballast mixtures was optimal for improving shear modulus with minimal decrease in the shear strength characteristics.
5. The TDRB-5 % mixture demonstrated superior damping properties in cyclic simple shear tests, indicating its capability to absorb and dissipate energy more effectively under cyclic loading conditions.
6. Using waste tire-derived aggregates for modifying recycled ballast material provides a sustainable approach to improving ballast performance and aligns with the environmental objectives of recycling industrial waste materials.

In summary, the findings from large-scale cyclic simple shear testing have contributed new understanding of ballast behavior under cyclic shear loads. It is recommended that reused ballast combined with 5 % by mass TDAs can notably enhance composite material performance, improving damping capacity, reducing degradation, and a relatively smaller reduction in shear strength.

Funding Information

LIAISON (HORIZON-CL5-2022-D6-02-06, GA 101103698). The Slovenian Research Agency (ARIS), Program group P2-0273.

CRediT authorship contribution statement

Stanislav Lenart: Writing – review & editing, Validation, Supervision, Resources, Project administration, Methodology, Investigation, Funding acquisition, Formal analysis, Data curation, Conceptualization. **Siva Ram Karumanchi:** Writing – original draft, Visualization, Validation, Software, Methodology, Investigation, Formal analysis, Data curation.

Declaration of competing interest

The authors declare that they have no known competing financial interests or personal relationships that could have appeared to influence the work reported in this paper.

Acknowledgments

The authors acknowledge the financial support provided by LIAISON (HORIZON-CL5-2022-D6-02-06, GA 101103698), and The Slovenian Research and Innovation Agency (ARIS) Program group P2-0273. The authors would like to thank the Ministry of Infrastructure, Directorate of Infrastructure of the Republic of Slovenia (DRSI), for their support during the project and Slovenian Railways – ŽGP for the provision of ballast material. The authors would also like to thank Mr. Marko Brodnik for his valuable support and encouraging approach during the sample preparation and experiments.

Data availability

Data will be made available on request.

References

[1] Profillidis V. Railway Management and Engineering. Routledge 2016. https://doi.org/10.4324/9781315245362.
[2] Sadeghi J, Askarinejad H. An investigation into the effects of track structural conditions on railway track geometry deviations. Proc Inst Mech Eng F J Rail Rapid Transit 2009;223:415–25. https://doi.org/10.1243/09544097JRRT266.
[3] Koohmishi M, Palassi M. Degradation of railway ballast under impact loading considering the morphological properties of aggregate. Transp Geotech 2020;25. https://doi.org/10.1016/j.trgeo.2020.100398.
[4] Prasad KVS, Hussaini SKK. Review of different stabilization techniques adapted in ballasted tracks. Constr Build Mater 2022;340. https://doi.org/10.1016/j.conbuildmat.2022.127747.
[5] Touqan M, Ahmed A, El Naggar H, Stark T. Static and cyclic characterization of fouled railroad sub-ballast layer behaviour. Soil Dyn Earthq Eng 2020;137. https://doi.org/10.1016/j.soildyn.2020.106293.
[6] Jing G, Qie L, Markine V, Jia W. Polyurethane reinforced ballasted track: Review, innovation and challenge. Constr Build Mater 2019;208:734–48. https://doi.org/10.1016/j.conbuildmat.2019.03.031.
[7] Gu Q, Zhao C, Bian X, Morrissey JP, Ooi JY. Trackbed settlement and associated ballast degradation due to repeated train moving loads. Soil Dyn Earthq Eng 2022;153. https://doi.org/10.1016/j.soildyn.2021.107109.
[8] Yu Z, Connolly DP, Woodward PK, Laghrouche O. Settlement behaviour of hybrid asphalt-ballast railway tracks. Constr Build Mater 2019;208:808–17. https://doi.org/10.1016/j.conbuildmat.2019.03.047.
[9] Indraratna B, Nimbalkar S, Christie D, Rujikiatkamjorn C, Vinod J. Field Assessment of the Performance of a Ballasted Rail Track with and without Geosynthetics. J Geotech Geoenviron Eng 2010;136:907–17. https://doi.org/10.1061/(asce)gt.1943-5606.0000312.
[10] Indraratna B, Babar Sajjad M, Ngo T, Gomes Correia A, Kelly R. Improved performance of ballasted tracks at transition zones: A review of experimental and modelling approaches. Transp Geotech 2019;21. https://doi.org/10.1016/j.trgeo.2019.100260.
[11] Qiang W, Jing G, Connolly DP, Aela P. The use of recycled rubber in ballasted railway tracks: A review. J Clean Prod 2023;420. https://doi.org/10.1016/j.jclepro.2023.138339.
[12] Indraratna B, Biabani MM, Nimbalkar S. Behavior of Geocell-Reinforced Subballast Subjected to Cyclic Loading in Plane-Strain Condition. J Geotech Geoenviron Eng 2015;141. https://doi.org/10.1061/(asce)gt.1943-5606.0001199.
[13] Leshchinsky B, Ling HI. Numerical modeling of behavior of railway ballasted structure with geocell confinement. Geotext Geomembr 2013;36:33–43. https://doi.org/10.1016/j.geotexmem.2012.10.006.
[14] Biabani MM, Ngo NT, Indraratna B. Performance evaluation of railway subballast stabilised with geocell based on pull-out testing. Geotext Geomembr 2016;44:579–91. https://doi.org/10.1016/j.geotexmem.2016.03.006.
[15] Li L, Cheng B, Xiao H, Li W, Huang S. Dynamic mechanical performance of geogrid–waste tyre-reinforced railway ballast under cyclic loading. Constr Build Mater 2024;411. https://doi.org/10.1016/j.conbuildmat.2023.134470.
[16] Karumanchi SR, Lenart S, Ghafoori Y, Garcia SD. Rubber Modified Ballasted Track Systems for Low Noise and Low Vibration 2024:1–8. https://doi.org/10.4203/ccc.7.13.7.
[17] Indraratna B, Sun Q, Grant J. Behaviour of subballast reinforced with used tyre and potential application in rail tracks. Transp Geotech 2017;12:26–36. https://doi.org/10.1016/j.trgeo.2017.08.006.
[18] Rao GV, Dutta RK. Compressibility and strength behaviour of sand-tyre chip mixtures. Geotech Geol Eng 2006;24:711–24. https://doi.org/10.1007/s10706-004-4006-x.
[19] Sol-Sánchez M, Moreno-Navarro F, Rubio-Gámez MC. Viability of using end-of-life tire pads as under sleeper pads in railway. Constr Build Mater 2014;64:150–6. https://doi.org/10.1016/j.conbuildmat.2014.04.013.
[20] Ngo T, Indraratna B. Mitigating ballast degradation with under-sleeper rubber pads: Experimental and numerical perspectives. Comput Geotech 2020;122. https://doi.org/10.1016/j.compgeo.2020.103540.
[21] Jayasuriya C, Indraratna B, Ngoc NT. Experimental study to examine the role of under sleeper pads for improved performance of ballast under cyclic loading. Transp Geotech 2019;19:61–73. https://doi.org/10.1016/j.trgeo.2019.01.005.
[22] Esmaeili M, Farsi S, Shamohammadi A. Effect of rock strength on the degradation of ballast equipped with under sleeper pad. Constr Build Mater 2022;321. https://doi.org/10.1016/j.conbuildmat.2022.126413.
[23] Kraśkiewicz C, Zbiciak A, Wasilewski K, Al S-Z. Laboratory tests and analyses of the level of vibration suppression of prototype under ballast mats (Ubm) in the ballasted track systems. Materials 2021;14:1–18. https://doi.org/10.3390/ma14020313.
[24] Ngo TN, Indraratna B, Rujikiatkamjorn C. Improved performance of ballasted tracks under impact loading by recycled rubber mats. Transp Geotech 2019;20. https://doi.org/10.1016/j.trgeo.2019.04.002.
[25] Uranjek M, Štrukelj A, Lenart S, Peruš I. Analysis of influential parameters for accelerated degradation of ballast railway track. Constr Build Mater 2020;261. https://doi.org/10.1016/j.conbuildmat.2020.119938.
[26] Guo Y, Xie J, Fan Z, Markine V, Connolly DP, Jing G. Railway ballast material selection and evaluation: A review. Constr Build Mater 2022;344. https://doi.org/10.1016/j.conbuildmat.2022.128218.
[27] Lenart S, Kaynia AM. Dynamic properties of lightweight foamed glass and their effect on railway vibration. Transp Geotech 2019;21. https://doi.org/10.1016/j.trgeo.2019.100276.
[28] Wu H, Zhu L, Song W, Xu Z, Xu F, Gong H. Impact performance of ballast by incorporating waste tire-derived aggregates. Constr Build Mater 2021;288. https://doi.org/10.1016/j.conbuildmat.2021.122992.
[29] Fathali M, Nejad FM, Esmaeili M. Influence of Tire-Derived Aggregates on the Properties of Railway Ballast Material. J Mater Civ Eng 2017;29. https://doi.org/10.1061/(ASCE)MT.1943-5533.0001702.
[30] Sweta K, Hussaini SKK. Behavior evaluation of geogrid-reinforced ballast-subballast interface under shear condition. Geotext Geomembr 2019;47:23–31. https://doi.org/10.1016/j.geotexmem.2018.09.002.

[31] Sweta K, Hussaini SKK. Role of particle breakage on damping, resiliency and service life of geogrid-reinforced ballasted tracks. Transp Geotech 2022;37. https://doi.org/10.1016/j.trgeo.2022.100828.
[32] Hussaini SKK, Indraratna B, Vinod JS. Performance assessment of geogrid-reinforced railroad ballast during cyclic loading. Transp Geotech 2015;2:99–107. https://doi.org/10.1016/j.trgeo.2014.11.002.
[33] Abadi T, Madhusudhan BN, Li H, Le Pen L. Reusing Life-Expired Railway Ballast: Laboratory Testing, Shape Analysis, and Petrographic Evaluation. J Geotech Geoenviron Eng 2023;149. https://doi.org/10.1061/(asce)gt.1943-5606.0002904.
[34] Cabalar AF, Abdulnafaa MD, Isbuga V. Plate Loading Tests on Clay with Construction and Demolition Materials. Arab J Sci Eng 2021;46:4307–17. https://doi.org/10.1007/s13369-020-04916-6.
[35] Indraratna B, Mehmood F, Mishra S, Ngo T, Rujikiatkamjorn C. The role of recycled rubber inclusions on increased confinement in track substructure. Transp Geotech 2022;36. https://doi.org/10.1016/j.trgeo.2022.100829.
[36] Arachchige CMK, Indraratna B, Qi Y, Vinod JS, Rujikiatkamjorn C. Deformation and degradation behaviour of Rubber Intermixed Ballast System under cyclic loading. Eng Geol 2022;307. https://doi.org/10.1016/j.enggeo.2022.106786.
[37] Cabalar AF, Ismael IA, Yavuz A. Use of zinc coated steel CNC milling waste for road pavement subgrade. Transp Geotech 2020;23. https://doi.org/10.1016/j.trgeo.2020.100342.
[38] Sadeghi J, Toloukian A, Zarei MA, Khani N. Improvement of ballast behavior by inclusion of tire-derived aggregates with optimum size. Constr Build Mater 2025;458. https://doi.org/10.1016/j.conbuildmat.2024.139530.
[39] Qi Y, Indraratna B, Ngo T, Arachchige CMK, Hettiyahandi S. Sustainable solutions for railway using recycled rubber. Transp Geotech 2024;46. https://doi.org/10.1016/j.trgeo.2024.101256.
[40] Ebrahimi Alavijeh B, Mokhtari M, Aghaei AA. Behavior of fresh and recycled slag ballast under cyclic and post-cyclic monotonic loadings using large-scale triaxial tests. Soil Dyn Earthq Eng 2024;182:108720. https://doi.org/10.1016/j.soildyn.2024.108720.
[41] Indraratna B, Qi Y, Ngo T, Malisetty R, Arachchige CK. Innovative and cost-effective rail track construction using recycled rubber. Railway Eng Sci 2024. https://doi.org/10.1007/s40534-024-00352-6.
[42] Anjos R, Pinho-Lopes M, Powrie W. Effect of Crumb Rubber Size on the Packing of 1/3 Scaled. Ballast 2025:33–41. https://doi.org/10.1007/978-981-97-8237-6_4.
[43] Moussa A, El Naggar H, Sadrekarimi A. Dynamic characterization of tire derived aggregates using cyclic simple shear and bender element tests. Soil Dyn Earthq Eng 2023;165. https://doi.org/10.1016/j.soildyn.2022.107700.
[44] Zhang J, Yang N, Chen X, Hu H, Wang X, Zhang J. Investigation of the static and dynamic characteristics of TDA-subballast mixtures. Transp Geotech 2022;32. https://doi.org/10.1016/j.trgeo.2021.100676.
[45] Koohmishi M, Azarhoosh A. Stiffness and damping properties of railway ballast aggregate considering influence of degradation of aggregate and incorporation of crumb rubber. Soil Dyn Earthq Eng 2022;155. https://doi.org/10.1016/j.soildyn.2022.107177.
[46] Chen J, Gao R, Liu Y, Shi Z, Zhang R. Numerical exploration of the behavior of coal-fouled ballast subjected to direct shear test. Constr Build Mater 2021;273. https://doi.org/10.1016/j.conbuildmat.2020.121927.
[47] Song W, Huang B, Shu X, Wu H, Gong H, Han B, et al. Improving Damping Properties of Railway Ballast by Addition of Tire-Derived Aggregate. Transp Res Rec 2019;2673:299–307. https://doi.org/10.1177/0361198119839345.
[48] Gong H, Song W, Huang B, Shu X, Han B, Wu H, et al. Direct shear properties of railway ballast mixed with tire derived aggregates: Experimental and numerical investigations. Constr Build Mater 2019;200:465–73. https://doi.org/10.1016/j.conbuildmat.2018.11.284.
[49] McCartney JS, Ghaaowd I, Fox PJ, Sanders MJ, Thielmann SS, Sander AC. Shearing Behavior of Tire-Derived Aggregate with Large Particle Size. II: Cyclic Simple Shear. J Geotech Geoenviron Eng 2017;143. https://doi.org/10.1061/(asce)gt.1943-5606.0001781.
[50] Fox PJ, Thielmann SS, Sanders MJ, Latham C, Ghaaowd I, McCartney JS. Large-scale combination direct shear/simple shear device for tire-derived aggregate. Geotech Test J 2018;41:340–53. https://doi.org/10.1520/GTJ20160245.
[51] Esmaeili M, Zakeri JA, Ebrahimi H, Khadem SM. Experimental study on dynamic properties of railway ballast mixed with tire derived aggregate by modal shaker test. Adv Mech Eng 2016;8:1–13. https://doi.org/10.1177/1687814016640245.
[52] Sol-Sánchez M, Thom NH, Moreno-Navarro F, Rubio-Gámez MC, Airey GD. A study into the use of crumb rubber in railway ballast. Constr Build Mater 2015;75:19–24. https://doi.org/10.1016/j.conbuildmat.2014.10.045.
[53] Indraratna B, Lackenby J, Christie D. Effect of confining pressure on the degradation of ballast under cyclic loading. vol. 55. 2005.
[54] Sol-Sánchez M, Moreno-Navarro F, Martínez-Montes G, Rubio-Gámez MC. An alternative sustainable railway maintenance technique based on the use of rubber particles. J Clean Prod 2017;142:3850–8. https://doi.org/10.1016/j.jclepro.2016.10.077.
[55] Asadi M, Mahboubi A, Thoeni K. Discrete modeling of sand–tire mixture considering grain-scale deformability. Granul Matter 2018;20:18. https://doi.org/10.1007/s10035-018-0791-4.
[56] Lenart S, Koseki J, Miyashita Y, Sato T. Large-scale triaxial tests of dense gravel material at low confining pressures. Soils Found 2014;54:45–55. https://doi.org/10.1016/j.sandf.2013.12.005.
[57] Alabbasi Y, Hussein M. Large-scale triaxial and box testing on railroad ballast: a review. SN Appl Sci 2019;1. https://doi.org/10.1007/s42452-019-1459-3.
[58] Indraratna B, Ionescu D, Christie HD. Shear Behavior of Railway Ballast Based on Large-Scale Triaxial Tests. J Geotech Geoenviron Eng 1998;124:439–49. https://doi.org/10.1061/(asce)1090-0241(1998)124:5(439).
[59] Qian Y, Tutumluer E, Hashash YMA, Ghaboussi J. Triaxial testing of new and degraded ballast under dry and wet conditions. Transp Geotech 2022;34. https://doi.org/10.1016/j.trgeo.2022.100744.
[60] Ngo NT, Indraratna B, Ferreira FB, Rujikiatkamjorn C. Improved performance of geosynthetics enhanced ballast: Laboratory and numerical studies. Proc Inst Civ Eng Ground Improv 2018;171:202–22. https://doi.org/10.1680/jgrim.17.00051.
[61] Orosz Á, Farkas Z, Tamás K. Experimental investigation of mixing railway ballast grains with different form using large-scale direct shear box apparatus. Transp Geotech 2023;42. https://doi.org/10.1016/j.trgeo.2023.101105.
[62] Jia W, Markine V, Guo Y, Jing G. Experimental and numerical investigations on the shear behaviour of recycled railway ballast. Constr Build Mater 2019;217:310–20. https://doi.org/10.1016/j.conbuildmat.2019.05.020.
[63] Nålsund R, Tutumuler E, Horvli I. Degradation of railway ballast through large scale triaxial and full scale rail track model tests. Proceedings Ninth International Conference on the Bearing Capacity of Roads, Railways and Airfields 2013;2:1–14.
[64] Sevi A, Ge L. Cyclic Behaviors of Railroad Ballast within the Parallel Gradation Scaling Framework. J Mater Civ Eng 2012;24:797–804. https://doi.org/10.1061/(ASCE)MT.1943-5533.0000460.
[65] Moussa A, El Naggar H. Dynamic Characterization of Tire Derived Aggregates. J Mater Civ Eng 2021;33. https://doi.org/10.1061/(asce)mt.1943-5533.0003583.
[66] Fortunato E, Fontul S, Paixão A, Asseiceiro F. Case study on the rehabilitation of old railway lines: experimental field works. Proceedings Ninth International Conference on the Bearing Capacity of Roads, Railways and Airfields 2013;2:1–10.
[67] Fathali M, Chalabii J, Astaraki F, Esmaeili M. A new degradation model for life cycle assessment of railway ballast materials. Constr Build Mater 2021;270. https://doi.org/10.1016/j.conbuildmat.2020.121437.
[68] Kim J, Park BS, Woo SI, Choi YT. Evaluation of ballasted-track condition based on aggregate-shape characterization. Constr Build Mater 2020;232. https://doi.org/10.1016/j.conbuildmat.2019.117082.
[69] Moaveni M, Qian Y, Boler H, Mishra D, Tutumluer E. Investigation of Ballast Degradation and Fouling Trends using Image Analysis, n.d. DOI: 10.4203/ccp.104.123.
[70] Demir S, Cabalar AF. Undrained Triaxial Compression Testing of Sand-Low Plastic Silt Mixtures. Transp Geotech 2025;50. https://doi.org/10.1016/j.trgeo.2025.101482.
[71] Indraratna B, Ngo NT, Rujikiatkamjorn C. Deformation of Coal Fouled Ballast Stabilized with Geogrid under Cyclic Load. J Geotech Geoenviron Eng 2013;139:1275–89. https://doi.org/10.1061/(asce)gt.1943-5606.0000864.
[72] Maqbool S, Koseki J. Large-Scale Triaxial Tests to Study Effects of Compaction Energy and Large Cyclic Loading History on Shear Behavior of Gravel. Soils Found 2010;50:633–44. https://doi.org/10.3208/sandf.50.633.
[73] Nong ZZ, Park SS, Lee DE. Comparison of sand liquefaction in cyclic triaxial and simple shear tests. Soils Found 2021;61:1071–85. https://doi.org/10.1016/j.sandf.2021.05.002.
[74] Al Tarhouni MA, Hawlader B. Monotonic and cyclic behaviour of sand in direct simple shear test conditions considering low stresses. Soil Dyn Earthq Eng 2021;150. https://doi.org/10.1016/j.soildyn.2021.106931.
[75] EN 13450. Aggregates for railway ballast. 2013.
[76] Lackenby J, Indraratna B, McDowell G, Christie D. Effect of confining pressure on ballast degradation and deformation under cyclic triaxial loading. Géotechnique 2007;57:527–36. https://doi.org/10.1680/geot.2007.57.6.527.
[77] Indraratna B, Ngo T, Rujikiatkamjorn C, Ferreira F. Advancement of Rail Ballast Testing Methodologies and Design Implications. Geo-Congress 2020, Reston, VA: American Society of Civil Engineers; 2020, p. 355–63. DOI: 10.1061/9780784482797.035.
[78] Feng Z-Y, Sutter K. Dynamic Properties of Granulated Rubber/Sand Mixtures. Geotech Test J 2000;23:338–44. https://doi.org/10.1520/GTJ11055J.
[79] Indraratna B, Vinod JS, Lackenby J. Influence of particle breakage on the resilient modulus of railway ballast. Géotechnique 2009;59:643–6. https://doi.org/10.1680/geot.2008.T.005.